Matrix stiffness modulates infection of endothelial cells by *Listeria monocytogenes* via expression of cell surface vimentin

Effie E. Bastounis[1], Yi-Ting Yeh[2], and Julie A. Theriot[1,3,4]

[1] Department of Biochemistry, Stanford University School of Medicine, Stanford, California, USA

[2] Department of Bioengineering, University of California San Diego, La Jolla, California, USA

[3] Department of Microbiology and Immunology, Stanford University School of Medicine, Stanford, California, USA

[4] Howard Hughes Medical Institute, Stanford University School of Medicine, Stanford, California, USA

*To whom correspondence should be addressed: theriot@stanford.edu

Running title: Vimentin-mediated *Listeria monocytogenes* infection of endothelial cells

Keywords: *Listeria monocytogenes*, microvascular endothelial cells, matrix stiffness, polyacrylamide hydrogel, mechanotransduction, bacterial adhesion, focal adhesion kinase, cell surface vimentin

ABSTRACT

Extracellular matrix (ECM) stiffness is one of many mechanical forces acting on mammalian adherent cells that influence cellular function. We have addressed the open question of how ECM stiffness might alter the susceptibility of host cells to infection by bacterial pathogens. We manufactured hydrogels of varying physiologically-relevant stiffness and seeded human microvascular endothelial cells (HMEC-1) on them. We then infected HMEC-1 with the bacterial pathogen *Listeria monocytogenes* (Lm) and found that adhesion of Lm onto host cells increases monotonically with increasing matrix stiffness, an effect that requires the activity of focal adhesion kinase (FAK). We identified cell surface vimentin as a candidate surface receptor mediating stiffness-dependent adhesion of Lm to HMEC-1, and demonstrated that bacterial infection of these host cells is decreased when surface vimentin is perturbed. Our results provide the first evidence that ECM stiffness can mediate the susceptibility of host cells to bacterial infection.

15 **INTRODUCTION**

16 The extracellular environment of cells provides both chemical and mechanical stimuli to
17 influence cell behavior and function (Geiger et al., 2009, Chien et al., 2005). Extracellular matrix
18 stiffness (ECM), one of the many mechanical forces acting on cells, is an important determinant
19 of cellular behavior for most adherent mammalian cells (Gattazzo et al., 2014; Wells, 2008).
20 Cells can sense the stiffness of their matrix, which can vary over many orders of magnitude, and
21 accordingly alter their motility, adhesion, growth and differentiation (Discher et al., 2005;
22 Birukova et al., 2013). Yet the exact pathways whereby cells sense mechanical signals and
23 transduce them to generate biological signal cascades and specific cellular responses are not
24 yet fully understood (Trepat et al., 2008).

25 In the context of host-pathogen interactions, effects of matrix stiffness variation may be
26 most interesting for infectious agents that have the capacity to infect many different kinds of
27 tissues in the human body. One such agent is the food-borne facultative bacterial pathogen
28 *Listeria monocytogenes* (Lm). After initial invasion into the intestinal epithelium, Lm is able to
29 spread through the vasculature to distant organs, and can cause serious complications such as
30 meningitis and late-term spontaneous abortion by virtue of its unusual ability to penetrate and
31 cross a wide variety of endothelial barriers including the blood-brain barrier and the placenta
32 (Jackson et al., 2010; Vazquez-Boland et al., 2001). Lm has a broad range of susceptible host
33 animals, and uses multiple pathogenic strategies to achieve infection of a wide variety of tissues
34 within each host. It can directly adhere to and invade intestinal epithelial cells and hepatocytes
35 using bacterial surface proteins belonging to the internalin family, such as InlA, InlB and InlF,
36 which interact with host cell surface receptors (Mengaud et al., 1996; Shen et al., 2000; Kirchner
37 and Higgins, 2008). Lm can also directly adhere to and invade the vascular endothelial cells
38 (VECs) that line the inner lumen of blood vessels, using several distinct molecular mechanisms
39 that may vary depending on the subtype of VEC being infected (Drevets et al., 1995;

40 Greiffenberg et al., 1997; Wilson and Drevets, 1998; Greiffenberg et al., 1998; Parida et al.,
41 1998; Rengarajan et al., 2016).

42 Vascular endothelial cells (VECs) are known to be highly mechanosensitive. The
43 stiffness of the ECM surrounding blood vessels can vary significantly in space (location within
44 the vascular tree), in time (aging) and in pathophysiological conditions (e.g. arteriosclerosis,
45 cancer) (Chien et al., 2005; Collins et al., 2014; Krishnan et al., 2011; Volkman et al., 2002; Yeh
46 et al., 2012). These variations in stiffness can dramatically affect gene expression and barrier
47 integrity of VECs, thereby regulating the movement of vascular components from the
48 bloodstream into underlying tissues, including the dissemination of bacterial pathogens
49 (Lemichez et al., 2010). Clinical studies have shown that the local compliance of the basement
50 membrane of VECs in the brain tissue is as soft as 1 kPa, while bigger vessels such as the
51 aorta are as stiff as 20 kPa (Janmey and Miller, 2011; Kohn et al., 2015; Onken et al., 2014;
52 Wells, 2008; Wood et al., 2010), and their stiffness can increase up to 70 kPa due to aging
53 (Huynh et al., 2011) and in the context of cardiovascular diseases (CVDs), such as
54 atherosclerosis or hypertension (Blacher et al., 1999; Boutouyrie et al., 2002). VECs, like other
55 adherent cell types, probe features of their environment including its stiffness through integrins,
56 transmembrane receptors that allow attachment of the cells to their matrix through direct binding
57 to ECM ligand proteins (Schwartz, 2010; Senger et al., 2002). Integrin binding to the ECM leads
58 to recruitment of additional proteins and to formation of focal adhesions that in turn relay
59 information to the actin cytoskeleton and to various signaling molecules, modulating cellular
60 adhesion, shape, contractility, gene expression and fate in general (Pelham and Wang, 1997).
61 Focal adhesion kinase (FAK) is a non-receptor tyrosine kinase that has been established as a
62 key component of the signal transduction pathways triggered by integrins. The expression
63 and/or activity of FAK is dependent on ECM rigidity, showing decreased expression and/or
64 activation on softer matrices for certain cell types and can influence cell adhesion and motility
65 (Du et al., 2016; Higuita-Castro et al., 2014; Khatiwala et al., 2006; Provenzano et al., 2009).

66 However, no studies have previously addressed if and how VEC matrix stiffness sensing
67 through focal adhesions might affect host cells' interactions with bacterial pathogens.

68 Bacterial adhesion to the surface of cells is typically the initial event in the pathogenesis
69 of infection and can occur through receptor-mediated interactions between the host cell and the
70 pathogen (Pizarro-Cerdá and Cossart, 2006). Vimentin is generally an intracellular cytoskeletal
71 protein that forms intermediate filaments in many mesoderm-derived cells (Clarke and Allan,
72 2002). Vimentin can also be localized on the surface of cells for a variety of cell types, although
73 the precise mechanism whereby vimentin is delivered to the surface of cells is not yet fully
74 understood (Mitra et al., 2015; Mor-Vaknin et al., 2003; Päll et al., 2011; Rohrbeck et al., 2014;
75 Shigyo et al., 2015). Recent studies have shown that various bacteria as well as viruses use
76 surface vimentin as attachment receptor to facilitate entry into host cells (Bhattacharya et al.,
77 2009; Du et al., 2014; Garg et al., 2006; Mak and Brüggemann, 2016; Rohrbeck et al., 2014;
78 Yang et al., 2016; Yu et al., 2016; Zou et al., 2006). However, little is known about what
79 modulates the amount of vimentin exposed on the surface of cells and whether regulation of its
80 surface presentation potentially mediates bacterial uptake.

81 To assess whether ECM stiffness could mediate infection susceptibility of host cells, we
82 used Lm as our model pathogen and examined *in vitro* Lm infection in endothelial cells derived
83 from the microvasculature (human microvascular endothelial cells, HMEC-1) cultured on
84 matrices of varying stiffness. Subendothelial stiffness depends on the blood vessel's location
85 within the body, on the size of vessel, on age and on physiological or pathophysiological
86 conditions and so we chose our substrates' stiffness to span over a large range of stiffnesses,
87 from 0.6 kPa to 70 kPa (Kohn et al., 2015; Stroka and Aranda-Espinoza, 2011). We found a
88 two-fold increase in bacterial adhesion when cells reside on stiff as compared to soft matrices.
89 We also found that Tyr397 phosphorylation of FAK was higher for VECs residing on stiff
90 matrices, and furthermore that knockdown of FAK or treatment of VECs with FAK inhibitors led

91 to a decrease in bacterial infection. When we searched for candidate VEC surface receptors
92 differentially modulated depending on FAK activity, we identified surface vimentin as a
93 candidate, and found that decreasing the amount of host surface vimentin leads to a
94 concomitant decrease in Lm infection. Taken together, our findings provide evidence that
95 environmental stiffness of VECs, a previously unappreciated factor, plays an important role in
96 mediating infection susceptibility to Lm through differential activity of FAK that in turn affects the
97 amount of surface vimentin.

98 **RESULTS**

99 **Uptake of *Listeria monocytogenes* by HMEC-1 is more efficient when cells reside on stiff**
100 **substrates.**

101 Substrates on which vascular endothelial cells (VECs) are cultured *in vitro*, commonly
102 glass or tissue culture (TC) polystyrene, are approximately six orders of magnitude stiffer than
103 the natural ECM of human VECs (Dussurget et al., 2004; Sperling and Friedman, 1969). To be
104 able to recapitulate *in vivo* conditions and determine in a systematic way the effect of the VECs'
105 matrix stiffness on the efficiency of *Listeria monocytogenes* (Lm) infection, we developed an
106 assay based on manufacturing thin polyacrylamide hydrogels of varying stiffness ranging from
107 0.6 to 70 kPa on multi-well glass-bottom plates (Ahmed, 2015; Georges et al., 2006; Mih et al.,
108 2011) (Suppl. Fig. 1A). To enable cell adhesion, hydrogels were surface-coated with collagen I,
109 using a consistent density of collagen independent of hydrogel stiffness, as reported in previous
110 studies (Huang et al., 2013; Tse and Engler, 2010; Yeung et al., 2005). Human microvascular
111 endothelial cells (HMEC-1) seeded for 24 h on the hydrogels formed monolayers with
112 comparable densities regardless of substrate stiffness, similar to growth of these cells on TC
113 polystyrene (Suppl. Fig. 1B)

114 In order to measure the efficiency of bacterial infection quantitatively, we infected
115 HMEC-1 with a strain of Lm lacking expression of the ActA protein, which is necessary for intra-
116 and inter-cellular spread of this bacterium. In that way, we could attribute changes in the
117 number of infected cells directly to initial invasion events and not to spread of the bacteria from
118 cell to cell. We also confirmed that adhesion and invasion of wild-type Lm into HMEC-1 is
119 similar to that of Δ*actA* Lm, consistent with previous studies on other host cell types (Brundage
120 et al., 1993; Kocks et al., 1992), suggesting that ActA is not involved in adhesion or invasion
121 (Suppl. Fig. 1 D-F). The Δ*actA* Lm strain we used also expresses a fluorescent protein under a
122 promoter that is activated several hours after exposure of the bacteria to the host cell cytosol

123 (actAp::mTagRFP) (Zeldovich et al., 2011), allowing reliable fluorescence-based detection only
124 of bacteria that have successfully invaded the host cells. We determined the fraction of HMEC-1
125 infected with Lm in each well using flow cytometry (Fig. 1A-D). At a constant multiplicity of
126 infection (MOI) and constant host cell density, we found a monotonic increase (strictly
127 increasing relationship) in the number of VECs infected by Lm with increasing hydrogel stiffness
128 that was highly reproducible among biological replicates (Fig. 1E and Suppl. Fig 1C). The
129 overall efficiency of infection on the stiffest hydrogel substrates tested, 70 kPa, was comparable
130 to the efficiency of infection for the same cells grown on TC polystyrene, suggesting that above
131 a certain level of stiffness the infection efficiency does not change (Suppl. Fig 1C). Compared to
132 this maximum level of infection for HMEC-1 cultured on the stiffest substrates, infection
133 efficiency on the softest substrates decreased about two-fold (Fig. 1E and Suppl. Fig 1C).
134
135 **HMEC-1 on soft hydrogels show decreased FAK activity and decreased FAK activity**
136 **leads to less efficient Lm infection.**
137 Focal adhesion kinase (FAK) has been established as a key component of the signal
138 transduction pathways triggered by integrins binding to the ECM, and for some cell types FAK
139 expression and/or phosphorylation on residue Y397 have been shown to depend on mechanical
140 cues sensed by cells, such as shear stresses imposed by fluid flow and/or ECM rigidity (Du et
141 al., 2016; Higuita-Castro et al., 2014; Khatiwala et al., 2006; Mathieu et al., 2010; Provenzano et
142 al., 2009). We therefore sought to determine whether FAK expression or activity could be
143 modulated depending on the substrate stiffness where HMEC-1 reside. To that end, HMEC-1
144 were grown on soft 3 kPa hydrogels, stiff 70 kPa hydrogels and TC polystyrene substrates
145 treated with vehicle control or PF573228 FAK inhibitor. Cells were then harvested and total
146 amounts of FAK as well as pY397-FAK were determined using Western blot analysis. We found
147 that increasing the stiffness of the underlying substrate from 3 kPa to 70 kPa resulted in
148 increasing levels of pY397-FAK, but the levels of total FAK remained largely unchanged (Fig.

149 2A-C). In addition, the levels of pFAK-Y397 were similar for cells residing on stiff 70 kPa
150 hydrogels as compared to TC polystyrene substrates (Fig. 2A-C). Treating cells residing on
151 polystyrene with the specific FAK inhibitor PF573228 led to a significant decrease of pY397-
152 FAK while total FAK levels remained unchanged as compared to controls (Fig. 2A-C). Our
153 results suggest that FAK phosphorylation at Y397 is modulated by the stiffness of the substrate
154 on which HMEC-1 reside and therefore by different levels of cell–ECM interaction-induced focal
155 adhesion signaling.

156 To address whether reduced Lm uptake as observed for HMEC-1 residing on soft
157 matrices can be attributed at least in part to reduced FAK activity, we treated HMEC-1 residing
158 on polystyrene substrates with FAK inhibitors FAK-14 or PF573228 for one hour prior to
159 infection. We then measured the efficiency of infection with Lm as described above, and found
160 that both FAK inhibitors caused a similar dose-dependent inhibition of Lm infection (Fig. 2D).
161 We then transfected HMEC-1 with commercial non-targeting control siRNA (siNT) or siRNA
162 targeting FAK (siFAK) (Table S2) and total FAK expression was found to be about five-fold
163 reduced for the FAK knockdown cells as compared to controls as determined by
164 immunofluorescence (Suppl. Fig. 2A) and RT-PCR (Suppl Fig. 2B). We found a significant
165 approximately 2-fold decrease in Lm infection efficiency for the FAK knockdown cells as
166 compared to control cells (Fig. 2E; Suppl. Fig. 2C-D). Taken together these results are
167 consistent with the hypothesis that decreased bacterial infection of HMEC-1 residing on highly
168 compliant soft matrices may be in part due to decreased FAK activity.

169 To address whether elevating FAK activity can lead to increased bacterial uptake we
170 pre-treated cells for varying times with vasoconstrictor peptide hormone Angiotensin II, which
171 has been shown to induce an increase in phosphorylation of FAK *in vivo* in murine aortas (Louis
172 et al., 2007) and also shown *in vitro* to lead to enhanced phosphorylation of FAK at Y397 for a
173 variety of cell types (Greco et al., 2002; Torsoni et al., 2005; Weng and Shukla, 2002), including
174 endothelial cells (Montiel et al., 2005). We first treated HMEC-1 with 100 nM Angiotensin II for

175 varying times and then lysed the cells and used Western blotting to assess FAK expression and
176 phosphorylation of FAK at Y397 (Fig. 2F and Suppl. Fig. 2F). Interestingly, we found that
177 although FAK expression did not change upon treatment with Angiotensin II, phosphorylation of
178 FAK at Y397 increased substantially for cells treated with Angiotensin II for more than 30 min.
179 Since FAK activity was shown to be elevated for cells pretreated for more than 30 min with
180 Angiotensin II, we then asked whether that would be sufficient to lead to increased infection
181 susceptibility. When we infected HMEC-1 cells seeded on polystyrene substrates and
182 pretreated with 100 nM of Angiotensin II, we observed a modest but significant 23% increase in
183 infection susceptibility as compared to control cells (Fig. 2G and Suppl. Fig. 2E). We then
184 seeded HMEC-1 cells on soft 3 kPa and stiff 70 kPa hydrogels and pretreated cells with or
185 without 100 nM Angiotensin II for 2 h. We found a much stronger effect of Angiotensin II
186 increasing infection for cells plated on soft substrates than on stiff substrates; indeed, treatment
187 of cells on 3 kPa substrates with 100 nM Angiotensin II for 2 h was sufficient to raise the level of
188 infection to be approximately equal to infection on 70 kPa substrates (Suppl. Fig. 2G). This
189 result further supports the hypothesis that a primary determinant of the relatively inefficient
190 infection of HMEC-1 on soft substrates is the relatively low level of FAK activity in this
191 environmental condition.
192
193 **Adhesion but not invasion efficiency is increased when Lm infect HMEC-1 residing on**
194 **stiff substrates.**
195 Decreased infection efficiency of Lm in HMEC-1 residing on soft matrices or treated with
196 FAK inhibitors could be due to quantitative changes at several different steps in the infection
197 process, for example decreased bacterial adhesion onto HMEC-1, or decreased invasion of the
198 adhering bacteria into the HMEC-1, or a combination of both. To help identify the exact step in
199 infection that is sensitive to substrate stiffness, we used a constitutively GFP-expressing strain
200 of Lm to infect HMEC-1 residing on either soft 3 kPa hydrogels or stiff 70 kPa hydrogels, and

201 treated with vehicle control or PF573228. Samples were fixed shortly after infection and bacteria
202 that were attached to the cell surface but not yet internalized were specifically labeled with
203 antibodies under non-permeabilizing conditions. This inside/outside labeling method allows us
204 to distinguish between bacteria that are adhered but not internalized (GFP-positive and labeled
205 with the antibody) and those that are fully internalized by the HMEC-1 (GFP-positive but not
206 labeled with the antibody). We found that both the total number of bacteria per host cell and the
207 number of internalized bacteria per cell are significantly increased when HMEC-1 reside on stiff
208 70 kPa hydrogels as compared to soft 3 kPa hydrogels (Fig. 3A-B). However, importantly, the
209 invasion efficiency (ratio of internalized bacteria to total bacteria) did not differ between HMEC-1
210 residing on stiff as compared to soft matrices, suggesting that it is specifically the adhesion of
211 bacteria to the surface of host cells that is increased when the matrix stiffness is elevated and
212 which leads to increased Lm infection efficiency for cells residing on stiffer matrices (Fig. 3C).
213 Interestingly, we found a decrease in both Lm adhesion and invasion efficiency irrespective of
214 hydrogel stiffness for the cells treated with the FAK inhibitor (Fig. 3), suggesting that FAK
215 activity levels modulate both adhesion and invasion efficiency of Lm in HMEC-1, while substrate
216 stiffness affects adhesion only.
217
218 **InlB contributes to Lm infection of HMEC-1 but is not modulated by substrate stiffness**.
219 Our data indicate that lower FAK activity as it occurs when HMEC-1 are seeded on
220 softer hydrogels leads to decreased Lm adhesion onto the surface of HMEC-1. This finding led
221 us to hypothesize that a receptor at the surface of cells could be differentially regulated
222 depending on substrate stiffness, leading to decreased bacterial adhesion. To examine whether
223 any of the Lm internalins known to play a role in adhesion or invasion of other cell types,
224 including VECs, is implicated in infection of HMEC-1 and responsible for the matrix stiffness
225 dependent susceptibility to infection, we infected HMEC-1 with mutant strains deficient in each
226 of the internalin-encoding genes *inlA*, *inlB* or *inlF* (Fig. 4A and Table S1). We found a two-fold

227 decrease in bacterial infection when InlB was not present, suggesting that InlB is one of possibly
228 multiple bacterial factors that contribute to Lm infection of HMEC-1. In contrast to the effect of
229 the deletion in the *inlB* gene, deletion of *inlF* had no effect in bacterial infection of HMEC-1.
230 Deletion of *inlA* resulted in very modest but reproducible reduction in infection as reported
231 previously for human brain microvascular endothelial cells infected with Lm (Greiffenberg et al.,
232 1998).

233 The importance of InlB for initial invasion of Lm into HMEC-1 was further confirmed by
234 infecting HMEC-1 with a different strain that had deletions in both *inlB* and *actA* so that bacteria
235 could not spread from cell to cell. Consistent with our previous findings, we observed a two-fold
236 decrease in bacterial uptake for a series of different multiplicities of infection (MOI) when *inlB*
237 was knocked out (Fig. 4B). Importantly, bacteria carrying a deletion of *inlB* still exhibited a
238 strong monotonic dependence of infection efficiency on substrate stiffness (Fig. 4C). This
239 finding indicates that, while InlB contributes to some step in the infection of HMEC-1 by Lm, it is
240 not governing the step that is sensitive to substrate stiffness.

241 We confirmed this conclusion using four different lines of experimentation. First, we
242 directly assessed the effect of *inlB* deletion on bacterial adhesion and invasion of HMEC-1 using
243 inside/outside labeling as described above. We found that the total number of bacteria
244 associated with HMEC-1 cells was the same for wild-type bacteria as compared to an isogenic
245 *ΔinlB* strain (Fig. 4D), that is, adhesion to the host cell surface is indeed unchanged. However,
246 the number of internalized bacteria per cell and therefore the overall invasion efficiency was
247 significantly decreased for the *ΔinlB* strain (Fig. 4E-F). Second, we examined the effect of
248 inhibiting the host cell binding partner for InlB, the receptor tyrosine kinase Met (also known as
249 the hepatocyte growth factor receptor), on bacterial invasion. We confirmed that HMEC-1
250 express Met (Suppl. Fig. 3A), and then treated the cells with varying concentrations of the highly
251 selective Met inhibitor SGX-523 prior to infection (Buchanan et al., 2009). We found that only

252 uptake of the control Δ*actA* strain of Lm decreased with increasing concentration of SGX-523,
253 while uptake of the isogenic Δ*actA*/Δ*inlB* Lm did not change substantially as a function of SGX-
254 523 concentration (Fig. 4G). Third, when we then transfected HMEC-1 with commercial non-
255 targeting control siRNA (siNT) or siRNA targeting Met (siMet) and then infected HMEC-1 with
256 Lm, we found a significant 2-fold decrease in Lm infection efficiency for the Met knockdown cells
257 as compared to control cells (Fig. 4H; Suppl. Fig. 3B-C), while confirming that Met expression
258 was five-fold reduced for the Met knockdown cells as compared to controls through RT-PCR
259 (Suppl. Fig. 3D and Table S2). When we then infected transfected siNT and siMet HMEC-1 with
260 Δ*actA*/Δ*inlB* Lm, we found no significant difference in infection Lm uptake between the two
261 conditions, consistent with the previous results of cells pretreated or not with the SGX-523 (Fig.
262 4G and Suppl. Fig. 3E). These results confirm that InlB most likely contributes to Lm invasion
263 into HMEC-1 by interacting with host Met, as has been shown for other cell types (Bierne and
264 Cossart, 2002; Parida et al., 1998). However, Lm invasion into HMEC-1 treated with SGX-523
265 still retains a strong dependence on substrate stiffness (Fig. 4I), just as we found for the *ΔinlB*
266 strain. Fourth, we found that infection of HMEC-1 with the Δ*actA*/Δ*inlB* strain of Lm is still highly
267 sensitive to inhibition of FAK with PF573228, showing a dose-response curve that parallels that
268 of the control Δ*actA* strain (Fig. 4J).

269 So far we can conclude that substrate stiffness affects the adhesion of Lm to the surface
270 of HMEC-1 such that bacterial adhesion to host cells residing on soft substrates is about two-
271 fold less than to host cells residing on stiff substrates. The well-characterized InlB-Met
272 interaction appears to contribute to invasion of adherent bacteria into HMEC-1, and is
273 responsible for about half of the invasion efficiency for Lm infecting these cells, however this
274 interaction does not govern bacterial adhesion per se, is not sensitive to substrate stiffness, and
275 is orthogonal to the FAK signaling axis. We therefore sought to identify alternative possible host

276 cell receptors for adhesion of Lm to the surface of HMEC-1 that might be responsible for the
277 stiffness-dependent effects we consistently observe.
278
279 **Inhibiting FAK activity leads to a reduced amount of cell surface vimentin for HMEC-1.**
280 Since the decreased FAK activity associated with growth of HMEC-1 on softer hydrogels
281 leads to decreased Lm adhesion onto the surface of host cells, we attempted to identify
282 candidate host surface receptors whose amount is modulated by FAK activity and which
283 mediate bacterial adhesion. Since manufacturing soft and stiff PA hydrogels with large
284 dimensions is both technically challenging and costly, we instead grew cells on large TC
285 polystyrene plates and treated them with vehicle control or the FAK inhibitor PF573228. We
286 then biotinylated the cell surface-exposed proteins using membrane-impermeable EZ-Link
287 Sulfo-NHS-SS-Biotin and isolated them by affinity chromatography with streptavidin-agarose
288 beads (Fujimoto et al., 1992; Nunomura et al., 2005). Isolated surface proteins were then run in
289 2D-PAGE gels to allow separation of proteins according to both their isoelectric points and their
290 molecular weight (Elia, 2012). Gels were silver stained and comparison between gels was
291 performed by marking the spots that differed in intensity (Fig. 5A-B). We found a spot at
292 approximately 55 kDa consistently differing in two independent experiments between the control
293 sample and the sample treated with the FAK inhibitor PF573228 (see circles in Fig. 5A-B). In a
294 third replicate experiment of surface protein isolation, 2D-PAGE gels were Coomassie stained
295 and that specific 55 kDa spot that differed as a function of FAK inhibitor treatment was excised
296 and further analyzed by nanoliquid chromatography tandem mass spectrometry (nanoLC-
297 MS/MS). We identified this spot as the protein vimentin (accession number: gi|340219, Mascot
298 identification score: 788, number of identified peptides: 87, mass: 53752, isoelectric point: 5.05,
299 sequence coverage: 61%). Vimentin is a major component of the cytoskeleton forming
300 intermediate filaments, but exists also in soluble form and has been previously found to localize

301 at the cell surface for a wide variety of cells including VECs (Du et al., 2014; Fuchs and Weber,
302 1994; Mitra et al., 2015; Yu et al., 2016; Zou et al., 2006).
303 Given the high validity of identification, we sought to confirm whether vimentin is
304 expressed at the surface of HMEC-1 by performing immunostaining of non-permeabilized
305 HMEC-1 seeded on collagen I-coated glass substrates followed by epifluorescence imaging
306 (Fig. 6). For negative controls, cells were incubated with secondary antibody alone. The anti-
307 vimentin H-84 antibody stained the vimentin intermediate filaments of permeabilized cells very
308 well (Fig. 6A-B). Non-permeabilized cells showed surface staining of vimentin near cell-cell
309 junctions and very low background staining was observed for cells incubated with secondary
310 antibody alone (Fig. 6C-D). This localization confirmed that cell surface vimentin could be a
311 plausible candidate responsible for adhesion of Lm to HMEC-1.
312
313 **HMEC-1 surface vimentin contributes to Lm uptake.**
314 To determine whether surface vimentin specifically contributes to Lm adhesion and
315 thereby infection of HMEC-1, we used three independent methods to decrease the availability of
316 cell surface vimentin for bacterial adhesion. First, we pretreated HMEC-1 with varying
317 concentrations of H-84 anti-vimentin antibody prior to infection with Lm, and found a dose-
318 dependent decrease in infection efficiency (Fig. 7A). We found a maximum two-fold decrease in
319 Lm infection when incubating cells with 80 μg/ml anti-vimentin antibody, while increasing further
320 the concentration of the antibody did not lead to further decrease in Lm uptake (Suppl. Fig. 3A).
321 Second, HMEC-1 were transfected with commercial non-targeting control siRNA (siNT)
322 or siRNA targeting vimentin (siVIM) and total vimentin expression was found to be five-fold
323 reduced for the vimentin knockdown cells as compared to controls through RT-PCR and
324 reduced total vimentin expression was also confirmed through immunofluorescence (Suppl. Fig.
325 4A –B and Table S2). We found a significant decrease (about 30%) in Lm infection efficiency for

326 the vimentin knockdown cells as compared to control cells, while confirming that cell confluency
327 under both conditions was similar (Fig. 7B; Suppl. Fig. 4C-F).
328 Third, we treated HMEC-1 cells with varying concentrations of withaferin, a natural
329 product known to bind the soluble form of vimentin (Bargagna-Mohan et al., 2013; Bargagna-
330 Mohan et al.; Chi et al., 2010). We found a dose-dependent decrease in infection efficiency for
331 Lm in withaferin-treated cells, again finding a maximum two-fold decrease when cells were
332 treated with 5-10 μM of withaferin prior to infection (Fig. 7C). Higher concentrations of withaferin
333 disrupted HMEC-1 cell-substrate adhesion. Overall these results are consistent with the
334 hypothesis that cell surface vimentin is responsible for about half of the amount of adhesion of
335 Lm to the HMEC-1 surface, and that vimentin presentation on the cell surface is sensitive to
336 substrate stiffness.
337 As an additional control to confirm that anti-vimentin antibodies and withaferin treatment
338 inhibit Lm uptake due to effects on surface vimentin and not to non-specific effects, we
339 transfected HMEC-1 with commercial non-targeting control siRNA (siNT) or siRNA targeting
340 vimentin (siVIM) and then blocked cells for 1h with the H-84 anti-vimentin antibody. We then
341 infected the host cells with constitutively GFP-expressing Lm and fixed samples shortly after
342 infection. Through quantitative microscopy we observed no significant change in infection
343 susceptibility for vimentin knock-down cells blocked with anti-vimentin antibodies prior to
344 infection as compared to vimentin knock-downs alone, confirming that the antibodies inhibit
345 uptake due to effects on vimentin and not to non-specific effects (Suppl Fig. 4G). Similarly,
346 when HMEC-1 transfected with siNT or siVIM were pretreated with our without withaferin we
347 found a significant decrease in bacterial adhesion only for the control cells treated with
348 withaferin and not for the vimentin knock-down cells (Suppl Fig. 4H). Finally, we hypothesized
349 that if vimentin localizes at cell-cell junctions, and given that perturbing the amount of surface
350 vimentin leads to up to a 2-fold decrease in infection susceptibility, then we should expect that
351 when infecting HMEC-1 with Lm half of the bacteria should adhere at cell-cell junctions and half

352 of the bacteria could adhere anywhere else. Indeed, when we infected HMEC-1 with Lm, fixed
353 the samples and then immunostained for VE-cadherin as a proxy for cell-cell junctions (Suppl.
354 Fig. 5A), we observed that quite often bacteria were found adhering at cell-cell junctions. This
355 was not the case for vimentin knockdown cells where bacteria where found all across the apical
356 surface of cells (Suppl. Fig. 5B).

357 To examine any possible interaction between the contribution of vimentin-based
358 adhesion and the contribution of InlB/Met-based invasion of Lm infecting HMEC-1, we
359 pretreated HMEC-1 with withaferin or vehicle control and then infected with either Δ*actA* or
360 Δ*actA/* Δ*inlB* Lm over a range of multiplicities of infection (MOI). Consistent with our results
361 described above, we found a two-fold decrease in Lm uptake when cells were pretreated with
362 withaferin and infected with Δ*actA* Lm or when cells were not treated with withaferin but were
363 infected with Δ*actA/* Δ*inlB* Lm (Fig. 7D). When cells were both pretreated with withaferin and
364 infected with Δ*actA/* Δ*inlB* Lm, infection was decreased four-fold relative to control (Fig. 7D) , i.e.
365 InlB/Met and vimentin contribute independently to infection efficiency. However, under all
366 conditions there was still residual infection, suggesting that Lm uses additional strategies to
367 achieve uptake by HMEC-1, other than interactions with surface vimentin for bacterial adhesion
368 and with Met for increased bacterial internalization.

369

370 **Uptake of *Listeria innocua* but not carboxylated latex beads by HMEC-1 depends on cell**
371 **surface vimentin.**

372 Our results demonstrate that the vimentin-dependent adhesion of Lm to HMEC-1 is
373 sensitive to substrate stiffness and is not mediated by the bacterial internalins InlA, InlB, or InlF.
374 In order to gain insight into whether vimentin-based bacterial adhesion is a result of a non-
375 specific stickiness or a specific host-bacterium interaction, we measured the influence of cell
376 surface vimentin on adhesion of other bacteria and of non-biological particles. *Listeria innocua*
377 (Li) is a bacterium closely related to Lm that is considered non-pathogenic in that it lacks the

378 putative internalin family members and other virulence factors that Lm carries (Glaser et al.,
379 2001; Lauer et al., 2002). When we infected HMEC-1 with comparable loads of Lm and Li, we
380 found that adhesion of both bacteria is comparable (Fig. 8A). We also found that treating
381 HMEC-1 with FAK inhibitor PF537228 or blocking HMEC-1 with anti-vimentin antibody H-84
382 reduces adhesion of both Lm and Li onto HMEC-1 by similar amounts (Fig. 8A). Next, to
383 examine whether a bacterial factor common in Lm and Li could responsible for surface vimentin
384 mediated adhesion, we blocked HMEC-1 with anti-vimentin antibody and exposed cells to 2 μm
385 carboxylated latex beads, which are efficiently taken up by VECs. We found that uptake of
386 beads did not vary with antibody concentration and was identical to uptake of cells treated with
387 isotype control (Fig. 8B). Our results suggest that cell surface vimentin is a common receptor for
388 both Lm and Li in the context of adhesion to HMEC-1, but uptake of nonbiological particles such
389 as carboxylated latex beads does not depend on surface vimentin.
390
391

392 **DISCUSSION**

393 **Bacterial infection of VECs depends on the stiffness of the matrix on which cells reside.**

394 Our study provides the first evidence that ECM stiffness is a crucial determinant in
395 modulating susceptibility of host cells to infection by bacterial pathogens. Using HMEC-1 cells
396 as model host adherent cells and Lm as model bacterial pathogen, we demonstrated that host
397 cell susceptibility to Lm infection increases with increasing ECM stiffness. Mechanosensitive
398 cells, such as VECs, can "feel" a variety of physical cues such as fluid shear stresses, cyclic
399 mechanical strains, matrix stiffness and respond to them by altering their morphology, gene
400 expression and function (Kohn et al., 2015; Reinhart-King, 2008). Interestingly, many signaling
401 pathways involved in mechanotransduction are common irrespective of the exact mechanical
402 stimulus (Li et al., 1997; Zebda et al., 2012). For instance, exposure of VECs to laminar shear
403 stress leads to recruitment of FAK at focal adhesions and to an increase in the phosphorylation
404 at Y397 (Li et al., 1997). Consistent with FAK activity being sensitive to mechanical stimuli, we
405 found that FAK activity is increased when cells reside on stiffer matrices. Concurrently, we
406 observe a decrease in Lm uptake when FAK activity is reduced or inhibited. It is possible that
407 enhanced FAK activity for VECs exposed to shear stresses, might also lead to increased Lm
408 uptake, but this still remains to be investigated (Li et al., 1997). In our study, we only focused on
409 the effect of ECM stiffness on host cell infection susceptibility and did not consider in our model
410 additional mechanical cues that host cells experience (Shi and Tarbell, 2011). Based on our
411 findings and on recent studies on shear flow-exposed endothelial cells infected with pathogens
412 *B. burgdorferi* or *S. aureus*, we speculate that similar to matrix stiffness it is plausible that
413 additional mechanical cues could also play an important role in mediating susceptibility of
414 adherent host cells to bacterial infection (Claes et al., 2014; Niddam et al., 2017). Therefore, the
415 development of organotypic models for studying bacterial infection, that take into account all of
416 the different *in vivo* mechanical cues sensed by cells, is pertinent and will aid our emerging
417 understanding of the biomechanics of host-bacteria interactions as well as the design of more

418 effective therapeutic interventions that take into consideration the local cellular mechanical
419 micro-environment.
420 Our findings suggest that together with biochemical cues, the stiffness of the
421 environment where cells reside is an additional variable worth considering since it affects
422 cellular behavior and susceptibility to bacterial infection. In traditional studies of bacterial
423 infection of host cells' ECM stiffness is not taken into account and such studies are commonly
424 performed on non-physiological glass or polystyrene surfaces. Our study on how HMEC-1
425 interact with Lm when varying subendothelial stiffness was designed with the intent to mimic
426 variations that occur in physiological conditions depending on the precise anatomic location of
427 the vessel, in aging and during pathophysiological conditions such as cardiovascular disease
428 (Zieman et al., 2005) or cancer (Acerbi et al., 2015). Our lower range of subendothelial matrix
429 stiffness (0.6 kPa) could be relevant for the brain microvasculature where the blood vessel
430 microenvironment is very soft whereas stiffer values are more relevant for bigger vessels or
431 aged/diseased vasculature (Kohn et al., 2015; Stroka and Aranda-Espinoza, 2011). For
432 instance, clinical studies on arteries of atherosclerotic mice have shown that vessel stiffness for
433 diseased mice can increase from 5 kPa to up to 28 kPa (Kothapalli et al., 2012). Similarly, injury
434 can increase vessel stiffness as has been shown for injured femoral artery whose stiffness
435 increases from 3 kPa to 10 kPa (Klein et al., 2009). Finally, studies have shown that aging can
436 lead to significant vessel stiffening with studies suggesting that the aorta stiffness due to aging
437 can raise from 20 kPa to 70 kPa (Huynh et al., 2011). We showed that subendothelial stiffness
438 changes the amount of surface vimentin expressed by VECs, therefore affecting critically how
439 much host cells will be susceptible to bacterial infection. That is atherosclerotic vessels or aged
440 vessels might be more susceptible to infection based on our findings, while VECs lining healthy
441 and softer vessels should be less susceptible to infection by Lm. It is plausible that low degree
442 of stiffness might be a host mechanism to protect against infection. For the purpose of the
443 present study we just examined how subendothelial stiffness modulates bacterial adhesion on

444 previously uninfected VECs. However, it is very possible that once bacteria infect their hosts
445 they might have developed ways to circumvent such a host mechanism by somehow altering
446 matrix stiffness*, i.e.* by reprogramming host cells to alter their production of ECM proteins or
447 matrix-degrading enzymes, which could lead to alterations in subendothelial stiffness and
448 subsequently VEC biomechanics and contractility, critically impacting infection. Future studies
449 should address how host cell biomechanics change upon infection and how bacterial infection
450 changes susceptibility of host cells to further infection.
451
452 **Surface vimentin is a receptor for *Listeria* infection of VECs**.
453 We found that lower FAK activity as occurs when HMEC-1 are seeded on softer
454 hydrogels leads to decreased Lm and Li adhesion onto the surface of HMEC-1 and that is
455 attributable to lower levels of cell surface vimentin. The role of cell surface vimentin as an
456 attachment receptor facilitating bacterial or viral entry has been previously documented for other
457 pathogens (Bhattacharya et al., 2009; Du et al., 2014; Garg et al., 2006; Mak and Brüggemann,
458 2016; Rohrbeck et al., 2014; Yang et al., 2016; Yu et al., 2016; Zou et al., 2006). VEC surface
459 vimentin in particular has been shown to be the receptor for attachment of *E. coli* K1 and
460 multiple viruses (Das et al., 2011; Du et al., 2014; Koudelka et al., 2009; Yang et al., 2016; Zou
461 et al., 2006). We speculate that matrix stiffness of VECs might possibly also affect uptake of the
462 above viruses and bacteria, since the amount of surface vimentin is reduced when FAK activity
463 is decreased as in the case of cells residing on highly compliant matrices.
464 Bacterial adhesion to the surface of cells is commonly required as a precursor to
465 invasion (Lebrun et al., 1996; Lecuit et al., 2000). Our finding that both Lm and Li adhesion is
466 reduced when HMEC-1 are blocked with anti-vimentin antibodies suggests that the possible
467 bacterial binding partner of vimentin might be expressed in both bacterial species. Surface
468 vimentin has been shown to possess lectin-like activity binding N-acetylglucosamine (GlcNAc),
469 a sugar that is also commonly found as a component of bacterial cell envelopes (Ise et al.,

470 2010; Konopka, 2012). Specifically, GlcNAc is found decorating the wall teichoic acids of Lm
471 serotype 1/2a strains, such as the 10403S strain used in this study (Fiedler, 1988). That implies
472 that bacterial carbohydrate-binding to host cell surface vimentin might also be a plausible
473 specific interaction.
474
475 **Lm uses multiple pathogenic strategies to infect VECs, some of which are independent**
476 **of ECM stiffness.**
477 We identified that the Lm virulence factor InlB contributes to invasion of HMEC-1 cells,
478 mostly likely via its well-characterized interaction with the host cell receptor Met. Similarly, Lm
479 uptake is decreased by two-fold when Met is inhibited. However deletion of *inlB* and decrease of
480 Met activity by siRNA knockdown or by pharmacological inhibition do not affect the ability of the
481 infection process to respond to changes in substrate stiffness. When we infected HMEC-1 with
482 Δ*actA*/Δ*inlB* Lm after treating host cells with withaferin that binds to soluble vimentin, we found a
483 four-fold decrease in infection relative to controls, indicating that the vimentin-dependent and
484 InlB-dependent pathways contribute to infection independently of one another; however, even
485 when both pathways were blocked there was still residual Lm infection. This residual Lm
486 infection suggests that there are additional InlB-independent and vimentin-independent
487 mechanisms that Lm leverage to infect HMEC-1.
488 Increased Lm adhesion onto HMEC-1 residing on stiff matrices could be attributed to
489 multiple factors. In this work, we investigated the possibility of a receptor at the surface of host
490 cells being differentially regulated when FAK activity is increased, as in stiff matrices, and
491 identified cell surface vimentin as a well-supported candidate receptor. However, it is also
492 possible that additional factors might also lead to the decreased adhesion of Lm onto HMEC-1
493 residing on softer matrices. It is plausible that the cell surface glycans of HMEC-1 might be
494 differentially regulated depending on the stiffness of the environment. For example previous
495 studies have suggested both a positive correlation between FAK activity and the heparan

496 sulfate portion of the glycocalyx (Gopal et al., 2010; Liu et al., 2002) and between the heparan
497 sulfate portion of the glycocalyx and Lm adhesion onto enterocytes (Henry-Stanley et al., 2003).
498 Another possibility could be the differential regulation of biophysical or mechanical properties of
499 the host cells depending on matrix stiffness (e.g. cell cortical stiffness, surface roughness,
500 membrane tension). For instance, studies on adhesion of bacteria onto hydrogel surfaces have
501 shown that adherence is increased on stiffer hydrogels (Kolewe et al., 2015), suggesting that if
502 cells become stiffer on stiffer hydrogels, cellular stiffness alone could lead to increased bacterial
503 adhesion (Higuita-Castro et al., 2014; Tang et al., 2012).
504
505 **VEC origin and physical cues might explain discrepancy between previous studies on**
506 **VEC infection by Lm.**
507 The endothelial lining of blood vessels displays remarkable spatiotemporal heterogeneity
508 and the basis of these morphological and functional differences are still unclear (Aird, 2007;
509 Aird, 2012; Ingram et al., 2004). It is well documented that mechanical and chemical cues
510 relayed to VECs by their environment can alter both function and gene expression of VECs
511 found at different tissues (Aird, 2012; Kohn et al., 2015). However, even when VECs from
512 different origins are placed *in vitro* in the same biochemical and mechanical environment, they
513 can still exhibit unique characteristics and behaviors that are intrinsic to the cells themselves
514 and are not determined by differential culture or environmental conditions (Craig et al., 1998;
515 Ostrowski et al., 2014; Stroka and Aranda-Espinoza, 2011; Ye et al., 2014). For example, the
516 response of human umbilical cord endothelial cells (HUVEC) to changes in curvature or shear
517 stress is completely distinct as compared to that of human brain microvascular endothelial cells
518 (HBMEC) (Ye et al., 2014). In accordance with the differences these two cell types exhibit in
519 response to geometrical constraints or mechanical stimuli, studies have also shown differences
520 with respect to Lm infection. Past studies suggest that HBMEC infection by Lm depends on InlB
521 (Greiffenberg et al., 1998), while HUVEC uptake of Lm appears to be independent of both the

522 internalins InlA and InlB (Greiffenberg et al., 1997; Rengarajan et al., 2016). These studies are
523 not necessarily conflicting but suggest that bacterial infection of VECs depends upon both the
524 environment and the particular origin of VECs and therefore conclusions should refer to the
525 exact cell type and not to endothelial cells in general. Since many pathological processes occur
526 at the microvascular level of organs, we chose in this study to use HMEC-1 as our model for
527 VECs. However, extrapolation from results obtained for HMEC-1 infection by Lm to other VECs
528 should be performed with caution. In a similar analogy, although Lm uptake by HMEC-1
529 increases with increasing subendothelial stiffness that relationship could be different if HMEC-1
530 were infected with different bacterial pathogens. We speculate that the relationship between
531 ECM stiffness and susceptibility to infection is likely host cell- and pathogen- specific.
532 In conclusion, our results provide the first strong evidence that the local mechanical
533 environment and in particular the matrix stiffness of VECs regulates susceptibility of VECs to Lm
534 infection. The novel mechanosensitive pathway we identified suggests that increased ECM
535 stiffness sensed by VECs leads to enhanced FAK activity that augments the amount of vimentin
536 exposed at the surface of VECs. Increased amount of surface vimentin in turn increases Lm
537 adhesion and subsequent uptake by VECs. Our studies on the effect of ECM stiffness in
538 bacterial uptake of VECs can have other significant implications, since they provide an example
539 of how mechanotransduction can be exploited in biology and medicine facilitating the
540 development of therapeutic interventions against bacterial infections and other diseases.
541
542

543 **MATERIALS AND METHODS**

544 **Fabrication of thin two-layered polyacrylamide (PA) hydrogels on 24-well glass-bottom**
545 **dishes**

546 PA hydrogel fabrication was done as previously described with a few modifications for
547 the specific experiments (Bastounis et al., 2011; Bastounis et al., 2014; Georges et al., 2006;
548 Vincent et al., 2013). 24-well glass bottom plates (MatTek, P24G-1.5-13-F) were incubated for 1
549 h with 500 μL of 2 M NaOH. Wells were rinsed with distilled water, and 500 μL of 2% 3-
550 Aminopropyltriethoxysilane (Sigma, 919-30-2) in 95% ethanol were added to each well for 5
551 min. Wells were rinsed again with water and 500 μL of 0.5% gluteraldehyde was added in each
552 well for 30 min. Wells were rinsed with water and dried at 60°C. To prepare hydrogels of varying
553 stiffness, mixtures containing 3–10% acrylamide (Sigma, A4058) and 0.06–0.6% bis-acrylamide
554 (Fisher, BP1404-250) were prepared. Specifically, 0.6 kPa hydrogels contained 3% acrylamide
555 and 0.06% bis-acrylamide, 3 kPa hydrogels contained 5% acrylamide and 0.1% bis-acrylamide,
556 20 kPa hydrogels contained 8% acrylamide and 0.26% bis-acrylamide, and 70 kPa hydrogels
557 contained 10% acrylamide and 0.6% bis-acrylamide. For each stiffness, two mixtures were
558 prepared the second of which contained 0.03% 0.1 μm diameter fluorescent beads (Invitrogen,
559 F8803). Mixtures were then degassed for 15 min to remove oxygen, which inhibits acrylamide
560 polymerization.

561 First, 0.06% APS and 0.43% TEMED were added to the solutions containing no beads
562 to initiate polymerization and then 3.6 μL of the mixture was added at the center of each well,
563 capped with 12-mm untreated circular glass coverslips and allowed to polymerize for 20 min.
564 The coverslips were then lifted with a syringe needle with a small hook at its tip and then 2.4 μL
565 of the mixture containing tracer beads was added, sandwiched again with a 12-mm untreated
566 circular glass coverslip, gently pressed downwards by means of forceps, and allowed to
567 polymerize for 20 min. 50 mM HEPES pH 7.5 was added in the wells, and coverslips were
568 removed using the syringe needle and forceps. PA hydrogels were UV-sterilized for 1 h.

569 Hydrogels were then activated by adding 200 µL 0.5% w/v heterobifunctional crosslinker Sulfo-
570 SANPAH (ProteoChem, c1111) in 1% DMSO and 50 mM HEPES pH 7.5 on the upper surface
571 of the hydrogels and exposing to UV light for 10 min. After activation, the hydrogels were
572 washed with 50 mM HEPES pH 7.5 to remove excess crosslinker and were coated with 200 µL
573 of 0.25 mg/mL rat tail collagen I (Sigma-Aldrich, C3867) in 50 mM HEPES overnight at room
574 temperature. Prior to seeding cells, hydrogels were incubated with cell media to allow
575 equilibration for 30 min.
576
577 **HMEC-1 culture and infection with *Listeria monocytogenes* (Lm)**
578 Human microvascular endothelial cells (HMEC-1, generous gift from Welch lab, UC
579 Berkeley) were maintained in MCDB 131 medium (Fisher Sci Co, 10372-019) supplemented
580 with 10% FBS (GemBio, 900-108), 10 ng/mL epidermal growth factor (Sigma, E9644), 1 µg/mL
581 hydrocortisone (Sigma, H0888), and 2mM L-glutamine (Sigma, 56-85-9).
582 HMEC-1 were infected as previously described with the following modifications
583 (Rengarajan et al., 2016). The day prior to infection, host cells were seeded at a density of
584 $4x10^5$ cells/well for cells residing on wells of 24-well plates or at a density of $1x10^5$ cells/well for
585 cells residing on wells of 48-well plates, and grown for 24 h. Lm liquid cultures were started from
586 a plate colony, and grown overnight, shaking, at 30 °C in Brain Heart Infusion (BHI) media (BD,
587 211059) supplemented with 200 µg/mL streptomycin and 7.5 µg/mL chloramphenicol. The day
588 of the infection, the O.D.600 of the overnight cultures was measured and diluted to 0.1.
589 Samples were incubated for 2 h shaking, in the dark at 30^oC in BHI media supplemented with
590 200 µg/mL streptomycin and 7.5 µg/mL chloramphenicol to allow the O.D. 600 to reach 0.2-0.3
591 and let bacteria enter the logarithmic growth phase. Bacteria were then washed 3 times with
592 PBS to remove any soluble factors and infections were performed in normal growth media
593 (Reed et al., 2014).

594 To synchronize invasion, Lm diluted in normal growth media were added on the HMEC-1
595 cells and samples were spun for 10 min at 200 x g prior to incubation. After 30 min of incubation
596 at 37 °C, samples were washed 4 times in PBS and after an additional 30 min, media was
597 replaced with media supplemented with 20 µg/mL gentamicin. Multiplicity of infection (MOI) was
598 determined by plating bacteria at different dilutions, on BHI agar plates with 200 µg/mL
599 streptomycin and 7.5 µg/mL chloramphenicol and measuring the number of colonies formed 2
600 days post-infection. A similar approach was followed when HMEC-1 were infected with *Listeria*
601 *innocua* (Li), except that BHI plates with no antibiotics were used. All bacterial strains used in
602 these studied are indicated in Table S1.
603 Analysis of infection via flow cytometry was performed at 7-8 h after exposure, unless
604 otherwise stated. For drug exposure experiments, unless otherwise indicated, media was
605 removed from the cells and replaced with media containing either the drug or vehicle control 1 h
606 prior to infection or 30 min prior to infection for the case of withaferin. Cells were cultured in the
607 drug-containing media for 1 h after infection. 1 h post-infection cells were washed four times and
608 drug-free gentamicin-containing media was added to the cells.
609
610 **Antibodies and reagents**
611 Hoechst (Thermofisher, D1306) was dissolved at 1 mg/mL in dimethyl formamide
612 (DMSO) and used at 1:1000. Drugs were dissolved in DMSO (Sigma, D2650) at the stock
613 concentrations indicated: 10 mM FAK inhibitor-14 (FAK-14) (Tocris Bioscience, 3414), 100 mM
614 PF573228 (Tocris Bioscience, 3239), 20 mM SGX 523 (Tocris Bioscience *5356*), 42 mM
615 withaferin (Sigma-Aldrich, W4394). Primary antibody used for staining of extracellular Lm was
616 rabbit polyclonal anti-*Listeria* genus specific antibody (ABCAM, ab35132). Primary antibody
617 used for staining Li was goat polyclonal BacTrace anti-*Listeria* genus specific antibody
618 (SeraCare Life Sciences Inc., 01-90-90). For incubation of cells with vimentin antibodies prior to
619 infection or immunostaining of surface vimentin, rabbit polyclonal H-84 vimentin antibody (Santa

620 Cruz Biotechnologies, sc-5565) was used. For isotype controls, cells were incubated with rabbit
621 IgG (Sigma, I5006). For western blotting the following antibodies were used: rabbit polyclonal
622 phospho-FAK Tyr397 (ThermoFisher, 44-624G), mouse monoclonal anti-FAK (EMD Millipore,
623 05-182), rabbit monoclonal anti-Met (cMet) antibody (Abcam, ab51067), anti-GAPDH antibody
624 (Cell signaling, 140C10).
625
626 **Flow cytometry of HMEC-1 cells infected with Lm**
627 7-8 h post-infection, infected HMEC-1 cells were detached from the substrate by
628 incubating them for 10 min with a mixture of 200 μL of 0.25% trypsin-EDTA and 0.05%
629 collagenase (Sigma, C0130). Solutions in each well were pipetted up and down 6 times to
630 ensure single cell suspensions, and 200 μL of complete media was added to inactivate trypsin
631 in each well. Solutions were transferred into 5 mL polystyrene tubes with a 35-μm cell strainer
632 cap (Falcon, 352235) and then samples were immediately analyzed by flow cytometry on the
633 Scanford FACScan analyzer (Custom Stanford and Cytek upgraded FACScan). 10,000-20,000
634 cells were analyzed per each replicate. To ensure analysis of single cells, the bulk of the
635 distribution of cell counts was gated using the forward versus side scatter plot. This gating
636 strategy ensures that single cells are analyzed and debris or cell doublets or triplets are
637 eliminated from the analysis. A second gating step was then performed to exclude cells that
638 autofluoresce by measuring the fluorescence of control-uninfected cells and gating the
639 population of infected cells so to exclude autofluorescence.
640
641 **Immunostaining of extracellular adherent bacteria**
642 HMEC-1 cells residing on either PA hydrogel substrates or glass collagen I-coated
643 coverslips were infected as described above with a Lm strain that constitutively expresses GFP.
644 20 min post-infection, 1 μg/mL Hoechst (Thermofisher, D1306) was added in each well to stain
645 the cells' nuclei. 30 min post-infection cells were washed 4 times in PBS and fixed with a non-

646 permeabilizing fixative for differential immunostaining for 20 min at room temperature (Yam and
647 Theriot, 2004). Fixative contained 0.32 M sucrose, 10mM MES pH 6.1, 138 mM KCl, 3 mM
648 $MgCl_2$, 2 mM EGTA and 4% formaldehyde EM grade. Following a wash with PBS, samples
649 were blocked for 30 min with 5% BSA in PBS and then incubated with anti-Lm primary antibody
650 (Abcam ab35132) diluted 1:100 in PBS containing 2% BSA for 1 h. Samples were washed in
651 PBS 3 times and then incubated with Alexa Fluor 546 goat anti-rabbit secondary antibody
652 (Invitrogen A-11035) diluted 1:250 in PBS containing 2% BSA for 1 h. Samples were washed 3
653 times in PBS and stored in 1 mL PBS for imaging. N > 1000 cells were analyzed per condition.
654 For imaging, we used an inverted Nikon Diaphot 200 with a CCD camera (Andor Technologies)
655 and a 40X air Plan Fluor NA 0.60 or a 100X oil objective. The microscope was controlled by the
656 MicroManager software package (Edelstein et al., 2014). For differential immunostaining, all
657 "green" bacteria associated with individual cells were counted as adherent; bacteria that were
658 both "green" and "red" (due to antibody binding) were counted as non-internalized. Nuclei
659 number was identified running a custom-made script in MATLAB (Mathworks Inc.) and the CellC
660 software was used for enumeration of the bacteria (Selinummi et al., 2005). For characterization
661 of total bacteria adhering to host cells (Lm or Li), same procedure was followed with the
662 exception that cells were permeabilized for 5 min in 0.2% Triton-X in PBS. Primary antibody
663 used was goat polyclonal BacTrace anti-*Listeria* genus specific antibody.
664

665 **Immunostaining of surface vimentin**

666 HMEC-1 cells residing on glass collagen I-coated coverslips were incubated at 37°C for
667 30 min with H-84 anti-vimentin antibody in 1:10 dilution in media. Cells were then washed three
668 times in PBS and fixed in 4% formaldehyde (EM grade) in PBS for 10 min at room temperature.
669 A blocking step with 5% FBS in PBS was followed for 30 min and then cells were incubated with
670 secondary goat anti-rabbit AlexaFluor-546 antibody diluted 1:250 in PBS containing 2% BSA for
671 1 h. For negative controls to ensure label is specific to primary antibody, cells with no primary

672 antibody were fixed and incubated for 1 h with secondary goat anti-rabbit AlexaFluor-546
673 antibody. As an additional control, cells were also fixed, permeabilized and stained for
674 intracellular vimentin. For imaging, we used an inverted Nikon Diaphot 200 with a CCD camera
675 (Andor Technologies) and a 100X oil objective.
676
677 **HMEC-1 cell transfection with siRNA**
678 For each well of a 24-well plate, $6x10^4$ HMEC-1 cells suspended in serum free media
679 were reverse-transfected with siRNAs at 20 nM final concentration using 0.25 µL lipofectamine
680 RNAiMAX (Invitrogen 13778075). The transfection mix was replaced by full media 8 h later.
681 Synthetic siRNA pools (including 4 distinct siRNA sequences for each gene) to target vimentin,
682 Met and FAK were purchased from Dharmacon (Table S2). HMEC-1 cells were treated with
683 control (non-targeting, siGLO and Kif11) or experimental siRNA in accordance with the
684 manufacturer instructions. Specifically, to demonstrate that transfection performed was sufficient
685 to get siRNAs into the cells, we transfected cells with synthetic siRNA, siGLO, that makes cell
686 exposed to it fluorescent 24 h post-transfection (Table S2). In addition to track a cell cycle
687 phenotype to verify that knockdown has occurred with our protocol, we transfected cells with
688 siKif11 that results in substantial cell death of transfected cells, approximately 24-48 h post-
689 transfection and can be verified on the TC microscope. Bacterial infections were performed
690 approximately 72 h after transfection
691
692 **RT-qPCR**
693 HMEC-1 cells were treated with control or experimental siRNA as described above.
694 mRNA was harvested using the RNeasy Micro Kit (Qiagen, 74004) and cDNA was prepared
695 using the Superscript III First-strand Synthesis SuperMix (ThermoFisher, 18080–400). qPCR
696 was performed using TaqMan PreAmp Master (Thermofisher, 4331182). Genes of interest were
697 amplified using primers Hs00958113_g1 for Vimentin (ThermoFisher, 4331182) and

698 Hs99999905_m1 for GAPDH (ThermoFisher, 4333764) on a StepOnePlus Real-Time PCR
699 System. Normalized relative quantity (NRQ) and error were calculated as previously described
700 [92]. GAPDH was used as control gene.
701
702 **Western blotting of FAK and Met for HMEC-1 lysates coming from cells residing on**
703 **different substrates**
704 For assessing FAK and Met phosphorylation and expression levels, cells were seeded
705 on different substrates for 24 h, and then lysed with a buffer containing 1% Nonidet P-40, 0.5%
706 sodium deoxycholate, and a protease inhibitor mixture (PMSF, leupeptin, aprotinin, and sodium
707 orthovanadate). The total cell lysate was separated by SDS/PAGE (10% running, 4% stacking)
708 and transferred onto a nitrocellulose membrane (Immobilon P, 0.45-μm pore size). The
709 membrane was then incubated with the designated antibodies. Immunodetection was performed
710 using the Western-Light chemiluminescent detection system (Applied Biosystems).
711
712 **Cell surface protein isolation**
713 The isolation of cell surface proteins was adapted according to (Karhemo et al., 2012)
714 and (Roesli et al.). Cells were plated on 10 x 15 cm cell culture dishes until reaching confluency
715 for each condition. Cells from 10 dishes were incubated with vehicle control (DMSO) containing
716 media and cells from other 10 dishes with 2 μM PF537228 FAK inhibitor for 1 h. Cells were then
717 washed three times with DPBS+ (PBS, 0.901 mM CaCl2, 0.492 mM $MgCl_2$, 2.667 mM KCl, 1.47
718 mM KH_2PO_4, 137.931 mM NaCl, 8.060 mM Na_2HPO_4-$7H_2O$, 5.555 mM D-Glucose, 0.327 mM
719 Sodium Pyruvate), and incubated for 30 min with 0.5 mM EZ-Link Sulfo-NHS-SS-Biotin
720 (APExBIO, 21331) in DPBS+ at 4°C. To quench any non-reacted biotinylation, 1 M Tris pH 8.0
721 at a final concentration of 50 mM was added on each plate for 10 min at 4°C. The solution was
722 then discarded and plates were rinsed twice in 1X TBS (50 mM Tris-Cl pH 7.2, 150 mM NaCl). 2
723 ml of TBS pH 7.2 with 1X protease inhibitor cocktail (1 mM EDTA, 10 μM E-64, 2 μg/ml

724 leupeptin, 15 µg/ml benzamidine, 0.1 mM PMSF) and with 1X phosphatase inhibitor cocktail (1
725 mM Na_3VO_4, 1 mM NaF) were added to each dish and cells were scraped into 40 ml falcon
726 tubes. Tubes were spun at 400 x g for 5 min and the supernatant was discarded. 10 ml of lysis
727 buffer (50 mM Tris-HCL pH 8.5, 150 mM NaCl, 2% NP-40, 0.25% Deoxycholate, 2x protease
728 inhibitor cocktail, 1x osphatase inhibitor cocktail) were added to each single pellet obtained from
729 10 x 15 cm plates, and cells were passed through a 25 G needle attached to a 10-mL syringe 3
730 times. Lysates were then sonicated for 5 min in a bioruptor with 30 sec ON/OFF cycle. 1 mM
731 $MgCl_2$ and 50 U/ml benzonase (Sigma, 9025-65-4) were added to the samples that were then
732 incubated at 4 °C for 2 h on a rotator. EDTA to a final concentration of 5 mM was added to each
733 sample and samples were spun in an ultracentrifuge (Rotor type 70.1 Ti; 33,000 rpm) at
734 100,000 x g for 60 min at 4 °C. Supernatants were then transferred into fresh 15 mL Falcon
735 tubes and protein concentration was estimated by the BCA protein assay (Thermo Fisher
736 Scientific, Pierce Rockford). Equal amounts of protein (~5 mg) from each extract were used for
737 cell surface protein isolation.
738 Streptavidin agarose beads (Pierce, 20347) were washed three times with lysis buffer.
739 50 µL per 5 mg/lysate were added for 2 h or overnight at 4 °C on a rotator. Samples were then
740 transferred to 2 ml gravity flow columns (BioRad) pre-equilibrated with 2 ml wash buffer I (50
741 mM Tris-HCL pH 8.5, 150 mM NaCl, 2% NP-40, 0.25% Deoxycholate, 0.5% SDS). The flow-
742 through was collected and stored at -80 °C. Columns were washed once with 2 mL lysis buffer
743 (excluding protease and phosphatase inhibitors), then with 2 mL wash buffer I, followed by a 2
744 ml wash with wash buffer II (50 mM Tris-HCL pH 8.5, 300 mM NaCl, 2% NP-40, 0.25%
745 Deoxycholate, 0.5% SDS) and then again with 2 mL wash buffer I. Beads were then transferred
746 to a fresh 1.5 mL Eppendorf tube and 3x volume of elution buffer (100 mM Tris-HCl pH 8.5, 2%
747 SDS, 100 mM DTT) was added and samples were incubated at 37 °C for 1 h on a thermomixer.
748 Beads were then spun down and supernatant was collected and 5% aliquoted for gel-analysis

749 (2.5% elution for Western Blot and 2.5% elution for Silver staining of 1D-PAGE gels) and the
750 rest was put in a fresh 1.5 mL Eppendorf tube and stored at -80°C.
751
752 **2D SDS-PAGE electrophoresis and staining**
753 Two-dimensional electrophoresis was performed according to the carrier ampholyte
754 method of isoelectric focusing (Burgess-Cassler et al., 1989; O'Farrell, 1975) by Kendrick Labs,
755 Inc. (Madison, WI) as follows: Isoelectric focusing was carried out in a glass tube of inner
756 diameter 2.3 mm using 2% pH 3-10 Isodalt Servalytes (Serva, Heidelberg, Germany) for 9600
757 volt-h. 1 µg of an IEF internal standard, tropomyosin, was added to the sample. This protein
758 migrates as a doublet with lower polypeptide spot of MW 33,000 and pI 5.2. The enclosed tube
759 gel pH gradient plot for this set of Servalytes was determined with a surface pH electrode. After
760 equilibration for 10 min in Buffer 'O' (10% glycerol, 50 mM dithiothreitol, 2.3% SDS and 0.0625
761 M Tris, pH 6.8), each tube gel was sealed to the top of a stacking gel that overlaid a 10%
762 acrylamide slab gel (0.75 mm thick). SDS slab gel electrophoresis was carried out for about 4 h
763 at 15 mA/gel. The following proteins (Sigma Chemical Co., St. Louis, MO and EMD Millipore,
764 Billerica, MA) were used as molecular weight standards: myosin (220,000), phosphorylase A
765 (94,000), catalase (60,000), actin (43,000), carbonic anhydrase (29,000) and lysozyme
766 (14,000). These standards appear along the basic edge of the silver-stained (Oakley et al.,
767 1980) 10% acrylamide slab gel. The gels were dried between sheets of cellophane with the acid
768 edge to the left.
769
770 **Manual comparisons of patterns of silver-stained 2D gels**
771 Each gel for comparison was overlaid with a transparent sheet for labeling polypeptide
772 spot differences without marking the original gel. Two experienced analysts manually compared
773 protein patterns and polypeptide spots that were unique to or differed between controls and
774 PF537228 samples were outlined.

775

776 **Protein digestion and peptide extraction**

777 Proteins that were separated by SDS-PAGE/2D-PAGE and stained by Coomassie dye
778 were excised, washed and the proteins from the gel were treated according to published
779 protocols (Darie et al., 2011; Shevchenko et al., 1996; Sokolowska et al., 2012c). Briefly, the gel
780 pieces were washed in high purity, high performance liquid chromatography HPLC grade water,
781 dehydrated and cut into small pieces and de-stained by incubating in 50 mM ammonium
782 bicarbonate, 50 mM ammonium bicarbonate/50% acetonitrile, and 100% acetonitrile under
783 moderate shaking, followed by drying in a speed-vac concentrator. The gel bands were then
784 rehydrated with 50 mM ammonium bicarbonate. The procedure was repeated twice. The gel
785 bands were then rehydrated in 50 mM ammonium bicarbonate containing 10 mM DTT and
786 incubated at 56 ^{o}C for 45 min. The DTT solution was then replaced by 50 mM ammonium
787 bicarbonate containing 100 mM Iodoacetamide for 45 min in the dark, with occasional vortexing.
788 The gel pieces were then re-incubated in 50 mM ammonium bicarbonate/50% acetonitrile, and
789 100% acetonitrile under moderate shaking, followed by drying in speed-vac concentrator. The
790 dry gel pieces were then rehydrated using 50 mM ammonium bicarbonate containing 10 ng/μL
791 trypsin and incubated overnight at 37 ^{o}C under low shaking. The resulting peptides were
792 extracted twice with 5% formic acid/50 mM ammonium bicarbonate/50% acetonitrile and once
793 with 100% acetonitrile under moderate shaking. Peptide mixture was then dried in a speed-vac,
794 solubilized in 20 μL of 0.1% formic acid/2% acetonitrile.

795

796 **Liquid chromatography and tandem mass spectrometry (LC-MS/MS)**

797 The peptide mixture was analyzed by reverse phase liquid chromatography (LC) and MS
798 (LC-MS/MS) using a NanoAcuity UPLC (Micromass/Waters, Milford, MA) coupled to a Q-TOF
799 Ultima API MS (Micromass/Waters, Milford, MA), according to published procedures (Darie et
800 al., 2011; Sokolowska et al., 2012a; Sokolowska et al., 2012b; Spellman et al., 2008). Briefly,

801 the peptides were loaded onto a 100 μm x 10 mm NanoAquity BEH130 C18 1.7 μm UPLC
802 column (Waters, Milford, MA) and eluted over a 150 min gradient of 2-80% organic solvent
803 (ACN containing 0.1% FA) at a flow rate of 400 nL/min. The aqueous solvent was 0.1% FA in
804 HPLC water. The column was coupled to a Picotip Emitter Silicatip nano-electrospray needle
805 (New Objective, Woburn, MA). MS data acquisition involved survey MS scans and automatic
806 data dependent analysis (DDA) of the top three ions with the highest intensity ions with the
807 charge of 2+, 3+ or 4+ ions. The MS/MS was triggered when the MS signal intensity exceeded
808 10 counts/sec. In survey MS scans, the three most intense peaks were selected for collision-
809 induced dissociation (CID) and fragmented until the total MS/MS ion counts reached 10,000 or
810 for up to 6 sec each. The entire procedure used was previously described (Darie et al., 2011;
811 Sokolowska et al., 2012a; Sokolowska et al., 2012b). Calibration was performed for both
812 precursor and product ions using 1 pmol GluFib (Glu1-Fibrinopeptide B) standard peptide with
813 the sequence EGVNDNEEGFFSAR and the monoisotopic doubly-charged peak with m/z of
814 785.84.
815
816 **LC-MS/MS data processing and protein identification**
817 The raw data were processed using ProteinLynx Global Server (PLGS, version 2.4)
818 software as previously described (Sokolowska et al., 2012a). The following parameters were
819 used: background subtraction of polynomial order 5 adaptive with a threshold of 30%, two
820 smoothings with a window of three channels in Savitzky-Golay mode and centroid calculation of
821 top 80% of peaks based on a minimum peak width of 4 channels at half height. The resulting pkl
822 files were submitted for database search and protein identification to the public Mascot
823 database search (www.matrixscience.com, Matrix Science, London, UK) using the following
824 parameters: databases from NCBI (bacteria), parent mass error of 1.3 Da, product ion error of
825 0.8 Da, enzyme used: trypsin, one missed cleavage, propionamide as cysteine fixed
826 modification and Methionine oxidized as variable modification. To identify false negative results,

827 we used additional parameters such as different databases or organisms, a narrower error
828 window for the parent mass error (1.2 and then 0.2 Da) and for the product ion error (0.6 Da),
829 and up to two missed cleavage sites for trypsin. In addition, the pkl files were also searched
830 against in-house PLGS database version 2.4 (www.waters.com) using searching parameters
831 similar to the ones used for Mascot search. The Mascot and PLGS database search provided a
832 list of proteins for each gel band. To eliminate false positive results, for the proteins identified by
833 either one peptide or a mascot score lower than 25, we verified the MS/MS spectra that led to
834 identification of a protein.
835
836 **Atomic force microscopy force-distance measurements for hydrogel stiffness**
837 **characterization**
838 AFM force-distance beating were performed on PA hydrogel samples in 50mM HEPES
839 pH 7.5 buffer with a Park NX-10 AFM (Park Systems, Santa Clara, CA) using commercial silicon
840 nitride cantilevers CP-PNP-SiO with a sphere tip (sQube, 0.08 N/m stiffness, sphere radius ~ 1
841 micron) and gold coating on the reflective side. Temperature has been kept at 37 ˚C throughout
842 the experiment. Tip calibration curves were performed on glass substrate surface, which was
843 considered infinitely hard for the soft tips used. Two approach-withdraw cycles were performed
844 per cell. Data analysis of FD curves and calculation of Young's modulus was performed using
845 XEI software (Park Systems, Santa Clara, CA) and SPIP software (Image Metrology, Hørsholm,
846 Denmark).
847
848 **Visualization and comparison of distributions**
849 Distributions were visualized by using boxplots with the features indicated below. Bold
850 black line parallel to the x-axis indicates the median (second quartile) of the distribution and
851 boxplot's notched section shows the 95% confidence interval around the median (Wilcoxon–
852 Mann–Whitney nonparametric test). Regular black lines extended vertically below and above

the medians represent the first and third quartiles of the distribution. Lines extending vertically from the boxplot (whiskers) represent the lowest datum within 1.5 IQR (interquartile range) of the lower quartile and the highest datum within 1.5 IQR of the upper quartile. Data points beyond the whiskers are considered outliers and displayed as circles. To assess whether the differences between the medians of two distributions are significant we run a nonparametric Wilcoxon rank sum test since the distributions are not normal. One or two asterisks denote statistically significant differences between the medians of two distributions (<0.05 or <0.01, respectively).

862 **AUTHOR CONTRIBUTIONS:**

863 E.E.B. and J.A.T. conceived the project and designed the experiments. E.E.B. performed
864 experiments and analyzed data. Y.Y. performed experiments. E.E.B. and J.A.T. wrote the
865 paper.

866

867 **ACKNOWLEDGEMENTS:**

868 Our thanks to M. Footer, R. Lamason, M. Rengaranjan, G. Skariah and members of the Theriot
869 Lab for discussions and experimental support. This work was supported by NIH R01AI036929
870 (J.A.T), HHMI (J.A.T) and the American Heart Association (E.E.B. and Y.Y.). Flow cytometry
871 was performed at the Stanford Shared FACS Facility and RT-qPCR was performed at the
872 Stanford PAN Facility.

873

874 **FIGURE LEGENDS**

875 **Figure 1. Uptake of Lm by HMEC-1 depends on the stiffness of the matrix on which cells**
876 **reside.**

877 HMEC-1 residing on PA hydrogels of varying stiffness coated with collagen I were infected with
878 Δ*actA* Lm (actAp::mTagRFP). Infection was analyzed by flow cytometry 7–8 h post infection.
879 Bacteria were added at a multiplicity of infection (MOI) between 30 to 50 bacteria per host cell.
880 **(A-D)** Histograms of the logarithm of bacterial fluorescence intensity per cell for HMEC-1 plated
881 on 0.6 kPa **(A)**, 3 kPa **(B)**, 20 kPa **(C)** and 70 kPa **(D)** PA hydrogels. Histograms for N=5
882 replicates are shown in different colors. Histogram of control uninfected cells is shown in purple.
883 Based on the autofluorescence of the control group a gate is defined (see black and red lines)
884 showing what is considered uninfected (left, black line) and infected (right, red line). **(E)**
885 Boxplots of percentage of HMEC-1 infected with Δ*actA* Lm versus hydrogel stiffness for the data
886 shown in panels A-D. Circles represent outliers, and the boxplots' notched sections show the
887 95% confidence interval around the median (Wilcoxon–Mann–Whitney test, for details about
888 boxplots see Materials and Methods). One or two asterisks denote statistically significant
889 differences between the medians of two distributions (<0.05 or <0.01, respectively; Wilcoxon
890 rank sum test).

891

892 **Figure 2. FAK activity of HMEC-1 residing on soft PA hydrogels is decreased, as is Lm**
893 **uptake.**

894 (**A)** Western blots from whole HMEC-1 lysates showing expression of phosphorylated FAK
895 (Tyr397) and total FAK for cells residing on soft gels (3 kPa), stiff gels (70 kPa) and TC
896 polystyrene substrates with or without 2 μM PF537228 FAK inhibitor. In each Western blot,
897 equal quantities of protein were loaded and equal loading was confirmed in relation to
898 glyceraldehyde 3-phosphate dehydrogenase (GAPDH) expression. In each case, the Western
899 blots shown are representative of 3 independent experiments. (**B-C)** Normalized ratio of

900 FAK/GAPDH **(B)** and pFAK (Tyr397)/GAPDH **(C)** for HMEC-1 residing on varying stiffness
901 substrates and treated or not with 2 μM PF537228 FAK inhibitor. Different color circles
902 correspond to data from 3 independent experiments. Black bars represent the mean of the 3
903 independent experiments. For each experiment values have been normalized relative to the
904 ratio for cells residing on polystyrene substrates. **(D)** Inhibition of bacterial uptake by FAK
905 inhibitors. FAK-14, PF573228 or vehicle control was added 1 h before addition of bacteria to
906 HMEC-1 residing on polystyrene substrates. Percentage of HMEC-1 infected with Δ*actA* Lm
907 (actAp::mTagRFP) as a function of inhibitor concentration (mean +/- SD, N = 4 replicates). x = 0
908 corresponds to cells treated with vehicle control. Inset shows the same data with concentration
909 on a log scale. Infection was analyzed by flow cytometry, 7–8 h after infection. MOI is 80.
910 Representative data come from 1 of 3 independent experiments. (**E)** Boxplots of percentage of
911 HMEC-1 infected with Δ*actA* Lm (actAp::mTagRFP) for cells treated either with non-targeting
912 siRNA (siNT) or FAK siRNA (siFAK) (means +/-S.D., 3 independent experiments and N=6
913 replicates per experiment). MOI is 60 (gray) or 20 (green). Circles represent outliers, and the
914 boxplots' notched sections show the 95% confidence interval around the median (Wilcoxon–
915 Mann–Whitney test, for details about boxplots see Materials and Methods). One or two asterisks
916 denote statistically significant differences between the medians of two distributions (<0.05 or
917 <0.01, respectively; Wilcoxon rank sum test). (**F)** Normalized ratio of pFAK (Tyr397)/GAPDH for
918 HMEC-1 residing on polystyrene substrates and treated for varying amount of time (min) with
919 100 nM Angiotensin-II. Different color circles correspond to Western blot data from 3
920 independent experiments. In each Western blot, equal quantities of protein were loaded and
921 equal loading was confirmed in relation to glyceraldehyde 3-phosphate dehydrogenase
922 (GAPDH) expression. Black bars represent the mean of the 3 independent experiments. For
923 each experiment values have been normalized relative to the ratio for untreated cells (t = 0 min).
924 (**E)** Boxplots of percentage of HMEC-1 infected with Δ*actA* Lm (actAp::mTagRFP) for cells pre-
925 treated for 2 h either with vehicle control or 100 nM Angiotensin-II (means +/-S.D., 3

926 independent experiments and N=4 replicates per experiment). One or two asterisks denote
927 statistically significant differences between the medians of two distributions (<0.05 or <0.01,
928 respectively; Wilcoxon rank sum test).
929
930 **Figure 3. Lm adhesion but not invasion efficiency is increased when HMEC-1 reside on**
931 **stiff hydrogels.**
932 HMEC-1 residing on soft (3 kPa) or stiff (70 kPa) PA hydrogels and treated with vehicle control
933 or 2 μM PF537228 FAK inhibitor were infected with Lm (constitutively expressing GFP) at an
934 MOI between 1.5 to 15. 30 min post-infection samples were fixed, and immunostained, and
935 infection was analyzed by microscopy followed by image processing. Boxplots show: (**A)** total
936 bacteria per cell; **(B)** internalized bacteria per cell; **(C)** invasion efficiency (ratio of internalized
937 bacteria to total bacteria); **(D)** cells in the field of view. Representative data come from 1 of 3
938 independent experiments. N=800-1000 cells were analyzed for each condition. Two asterisks
939 denote statistically significant differences between the medians of two distributions (<0.01;
940 Wilcoxon rank sum test).
941
942 **Figure 4. Infection of HMEC-1 by Lm is in part mediated by InlB in a manner independent**
943 **of matrix stiffness.**
944 (**A)** Percentage of HMEC-1 infected with Lm as a function of the logarithm of MOI (mean +/- SD,
945 N = 4 replicates). HMEC-1 were infected with the indicated strains: wild type (circle); Δ*inlA*
946 (square); Δ*inlB* (cross); Δ*inlF* (diamond) (actAp::mTagRFP). The frequency of infected HMEC-1
947 was determined by flow cytometry 7–8 h post infection. Representative data come from 1 of 3
948 independent experiments. (**B)** Percentage of HMEC-1 infected with Lm as a function of the
949 logarithm of MOI (mean +/- SD, N = 4 replicates). HMEC-1 were infected with the indicated
950 strains: Δ*actA* (black circle); Δ*actA/*Δ*inlB* (gray square) (actAp::mTagRFP). The frequency of
951 infected HMEC-1 was determined by flow cytometry 7–8 h post infection. Representative data

952 come from 1 of 3 independent experiments. **(C)** Boxplots of percentage of HMEC-1 infected with
953 Lm as a function of substrate stiffness (N = 5-6 replicates). HMEC-1 were infected with the
954 indicated Lm strains: Δ*actA* (gray); Δ*actA/*Δ*inlB* (black) (actAp::mTagRFP) at an MOI of 20.
955 Infection was analyzed by flow cytometry, 7–8 h after infection. Representative data come from
956 1 of 3 independent experiments. One or two asterisks denote statistically significant differences
957 between the medians of two distributions (<0.05 or <0.01, respectively; Wilcoxon rank sum test).
958 (**D-F)** HMEC-1 residing on collagen I-coated glass substrates were infected with Lm
959 (constitutively expressing GFP) or Δ*inlB* Lm at an MOI of 3.5. 30 min post-infection samples
960 were fixed, immunostained and infection was analyzed by microscopy followed by image
961 processing. Boxplots showing: (**D)** total bacteria per cell; **(E)** internalized bacteria per cell; **(F)**
962 invasion efficiency (ratio of internalized bacteria to total bacteria). For each condition, 500-550
963 cells were analyzed in total. **(G)** Percentage of HMEC-1 infected with Lm as a function of SGX-
964 523 Met inhibitor concentration (mean +/- SD, N = 4 replicates). SGX-523 or vehicle control was
965 added 1 h before addition of bacteria. HMEC-1 were infected with the indicated strains: Δ*actA*
966 (black circle); Δ*actA/*Δ*inlB* (gray square) (actAp::mTagRFP) at an MOI of 75. Infection was
967 analyzed by flow cytometry, 7–8 h after infection. Representative data come from 1 of 3
968 independent experiments. **(H)** Boxplots of percentage of HMEC-1 infected with Δ*actA* Lm
969 (actAp::mTagRFP) for cells treated either with non-targeting siRNA (siNT) or Met siRNA (siFAK)
970 (means +/-S.D., 3 independent experiments and N=6 replicates per experiment). MOI is 60
971 (gray) or 20 (green). Circles represent outliers, and the boxplots' notched sections show the
972 95% confidence interval around the median (Wilcoxon–Mann–Whitney test, for details about
973 boxplots see Materials and Methods). One or two asterisks denote statistically significant
974 differences between the medians of two distributions (<0.05 or <0.01, respectively; Wilcoxon
975 rank sum test). **(I)** Boxplots of percentage of HMEC-1 infected with Lm as a function of substrate
976 stiffness (N = 5-6 replicates). HMEC-1 were treated with vehicle control or 1 μM SGX-523 Met
977 inhibitor for 1 h prior to infection and then infected with Δ*actA* Lm (actAp::mTagRFP). Infection

978 was analyzed by flow cytometry, 7–8 h after infection. MOI is 20. Representative data come
979 from 1 of 3 independent experiments. **(J)** Percentage of HMEC-1 infected with Lm as a function
980 of PF537228 inhibitor concentration (mean +/- SD, N = 4 replicates). PF537228 or vehicle
981 control was added 1 h before addition of bacteria (see Suppl. Fig. 1D). HMEC-1 were infected
982 with the indicated strains: Δ*actA* (black circle); Δ*actA/*Δ*inlB* (gray square) (actAp::mTagRFP) at
983 an MOI of 75. Infection was analyzed by flow cytometry, 7–8 h after infection. Representative
984 data come from 1 of 3 independent experiments. Inset shows the same data with concentration
985 on a log scale.
986
987 **Figure 5. Lower FAK activity leads to reduced amount of cell surface vimentin.**
988 (**A-B)** 2D-PAGE gels of plasma membrane proteins of HMEC-1 grown on TC polystyrene
989 substrates treated for 1 h with vehicle control (**A)** or 2 μM PF537228 FAK inhibitor (**B).** pH
990 increases from left to right. Gels were silver stained and one isoelectric point marker
991 (tropomyosin), added to each sample as an internal standard, is marked with a black arrow. The
992 one spot that differed consistently between 3 independent experiments is indicated with a black
993 circle and corresponds to vimentin (55 kDa).
994
995 **Figure 6. Surface vimentin is localized along the periphery of HMEC-1.**
996 **(A-D)** Cells were stained for vimentin using the rabbit anti-vimentin H-84 antibody. For negative
997 controls, cells were stained with secondary anti-rabbit IgG antibody alone. Representative
998 phase image of cells (left column), image of the nuclei (middle column) and H-84 anti-vimentin
999 antibody fluorescence (right column) are shown for: (**A)** Permeabilized HMEC-1 strained for
1000 intracellular vimentin; (**B)** Permeabilized HMEC-1 incubated with anti-rabbit IgG alone as
1001 negative controls. (**C)** Non permeabilized HMEC-1 stained for surface vimentin; **(D)** Non
1002 permeabilized HMEC-1 incubated with anti-rabbit IgG alone as negative controls. Scale bar

1003 shown in white is 20 μm. White arrows point at the localization of surface vimentin at cell-cell
1004 junctions.
1005
1006 **Figure 7. Surface vimentin of HMEC-1 is implicated in Lm uptake.** (**A)** Decrease in bacterial
1007 uptake after blocking HMEC-1 with anti-vimentin antibody H-84. Barplots of percentage of
1008 HMEC-1 infected with Δ*actA* Lm (actAp::mTagRFP) as a function of antibody concentration
1009 (means +/-S.D. and N=6 replicates per experiment). Representative data come from 1 of 3
1010 independent experiments. Infection was analyzed by flow cytometry, 7–8 h after infection. (**B)**
1011 Barplots of percentage of HMEC-1 infected with Δ*actA* Lm (actAp::mTagRFP) for cells treated
1012 either with non-targeting siRNA (siNT) or vimentin siRNA (siVIM) (means +/-S.D., and N=6
1013 replicates per experiment). Representative data come from 1 of 3 independent experiments.
1014 MOI is 50 (black barplots) and 17 (gray barplots). (**C)** Decreased uptake of Lm when HMEC-1
1015 are treated with withaferin that captures soluble vimentin 30 min prior to infection. Barplots of
1016 percentage of HMEC-1 infected with Δ*actA* Lm (actAp::mTagRFP) as a function of withaferin
1017 concentration (means +/-S.D. and N=6 replicates per experiment). Representative data come
1018 from 1 of 3 independent experiments. Infection was analyzed by flow cytometry, 7–8 h after
1019 infection. (**D)** Percentage of HMEC-1 infected with Lm as a function of the logarithm of MOI
1020 (mean +/- SD, N = 4 replicates). HMEC-1 were infected with the indicated strains: Δ*actA* (black);
1021 Δ*actA/*Δ*inlB* (gray) (actAp::mTagRFP) and HMEC-1 were treated with vehicle control (circle) or
1022 withaferin (diamond) for 30 min prior to infection. The frequency of infected HMEC-1 was
1023 determined by flow cytometry 7–8 h post infection. Representative data come from 1 of 3
1024 independent experiments. MOI ranged from 50 to 120. One or two asterisks denote statistically
1025 significant differences between the medians of infection fraction of control versus all other
1026 groups (<0.05 or <0.01, respectively; Wilcoxon rank sum test).
1027
1028 **Figure 8. Blocking HMEC-1 with anti-vimentin antibody reduces Li adhesion onto HMEC-1**

1029 **but not uptake of beads.**

1030 **(A)** Boxplots showing the number of bacteria per cell, for HMEC-1 residing on glass substrates
1031 and treated with vehicle control, 2 μM PF537228 FAK inhibitor, or 80 μg/mL H-84 anti-vimentin
1032 antibody prior to infection. Cells were infected with Lm or Li at an MOI of 4. 30 min post-infection
1033 samples were fixed, immunostained and adhesion of bacteria was analyzed by microscopy
1034 followed by image processing. For each condition, 2300-2600 cells were analyzed in total and
1035 data refer to 1 of 2 independent experiments. Two asterisks denote statistically significant
1036 differences between the median values of control cells versus all other groups <0.01; Wilcoxon
1037 rank sum test). **(B)** HMEC-1 residing on TC polystyrene substrates and blocked for 1 h with
1038 varying concentrations of H-84 anti-vimentin antibody or isotype control were "infected" with 2
1039 μm beads at different concentrations. The frequency of micro-bead uptake by HMEC-1 was
1040 determined by flow cytometry 2 h post addition of beads. Plot shows percentage of cells that
1041 internalized beads as a function of the beads/cell added for different H-84 antibody
1042 concentrations (mean +/- SD, N = 4 replicates).

1043

1044 **SUPPORTING INFORMATION CAPTIONS**

1045 **Figure S1. Lm infection of VECs residing on hydrogels of varying stiffness.**

1046 **(A)** Young's moduli of hydrogels. Plot showing the expected Young's modulus of the hydrogels
1047 given the amount of acrylamide and bis-acrylamide used versus the Young's modulus
1048 measured through AFM (N=6). Stiffness of the 0.6 kPa could not be measured, as the
1049 hydrogels were very soft and adhered to the AFM tip. **(B)** Fraction of cells passed through the
1050 flow cell in 20 s for HMEC-1 residing on varying stiffness substrates. HMEC-1 were seeded on
1051 0.6 kPa, 3 kPa, 20 kPa and 70 kPa PA hydrogels as well as TC polystyrene substrates for 24 h
1052 at a starting concentration of $4x10^5$ cells per well for 24 h. Cells were then detached from their
1053 matrix and number of cells per well passed through the flow cell in 20 s was measured using a
1054 flow cytometry for cells coming from N=5-6 wells for each substrate stiffness. Results from 3
1055 independent experiments were combined and for each experiment values were normalized
1056 relative to the mean number of cells passed through the flow cell for cells residing on TC
1057 polystyrene substrates. No significant differences were detected. **(C)** Boxplots of normalized
1058 fraction of HMEC-1 infected with Δ*actA* Lm for cells residing on PA hydrogels of varying
1059 stiffness or TC polystyrene. Stiffness (kPa) of each substrate is indicated. Boxplots refer to data
1060 from 3 independent experiments, with N = 5-6 replicates per experiment. For each experiment
1061 values have been normalized relative to the mean infection level of cells residing on polystyrene
1062 substrates. (**D-F)** HMEC-1 residing on collagen I-coated glass substrates were infected with Lm
1063 (constitutively expressing GFP) or Δ*atcA* Lm at an MOI of 2.7. 30 min post-infection samples
1064 were fixed, immunostained and infection was analyzed by microscopy followed by image
1065 processing. Boxplots showing: (**D)** total bacteria per cell; **(E)** internalized bacteria per cell; **(F)**
1066 invasion efficiency (ratio of internalized bacteria to total bacteria). For each condition, 500-600
1067 cells were analyzed in total. Representative data come from 1 of 2 independent experiments.
1068 Circles represent outliers, and the boxplots' notched sections show the 95% confidence interval
1069 around the median (Wilcoxon–Mann–Whitney test, for details about boxplots see Materials and

1070 Methods). One or two asterisks denote statistically significant differences between the medians
1071 of two distributions (<0.05 or <0.01, respectively; Wilcoxon rank sum test).
1072
1073 **Figure S2. FAK-dependent decrease in bacterial uptake. (A)** HMEC-1 treated with 20 nM of
1074 non-targeting siRNA (siNT, first row**)** or FAK siRNA (siFAK, second row**)** were stained for FAK
1075 using an anti-FAK antibody. Representative phase image of cells (left column), superimposed
1076 with the image of the nuclei (blue) and anti-FAK antibody fluorescence (purple, right column) are
1077 shown. Scale bar shown in white is 23 μm. **(B)** Relative with respect to GAPDH gene
1078 expression of FAK obtained by RT-qPCR. The levels relative levels of expression in each siRNA
1079 treated sample (#1-#3) are expressed relative to the control siNT treated sample #2 (normalized
1080 relative quantity, NRQ). N=3 replicates are shown for each group treated with either siNT or
1081 siVIM. (**C-D)** Histograms of the logarithm of Lm fluorescence intensity per cell for HMEC-1
1082 treated with 20 nM of non-targeting siRNA (siNT) **(C)** or FAK siRNA (siFAK) **(D)**. HMEC-1 were
1083 infected with *ΔactA* Lm (actAp::mTagRFP) and infection was analyzed by flow cytometry, 7–8 h
1084 after infection. MOI is 45. Histograms for N=6 replicates are shown in different colors. Control
1085 uninfected cells' histogram is shown in purple. Based on the autofluorescence of the control
1086 group a gate is defined (see black and red lines) showing what is considered uninfected (left,
1087 black line) and infected (right, red line). **(E)** Increase in bacterial uptake by Angiotensin II.
1088 Angiotensin II or vehicle control was added 2 h before addition of bacteria to HMEC-1 residing
1089 on polystyrene substrates. Percentage of HMEC-1 infected with Δ*actA* Lm (actAp::mTagRFP)
1090 as a function of inhibitor concentration (mean +/- SD, N = 4 replicates). Infection was analyzed
1091 by flow cytometry, 7–8 h after infection. MOI is 70. **(F)** Western blots from whole HMEC-1
1092 lysates showing expression of phosphorylated FAK (Tyr397) and total FAK for cells residing on
1093 TC polystyrene substrates and treated for varying amount of time with 100 nM Angiotensin-II. In
1094 each Western blot, equal quantities of protein were loaded and equal loading was confirmed in
1095 relation to glyceraldehyde 3-phosphate dehydrogenase (GAPDH) expression. The Western

1096 blots shown are representative of 3 independent experiments. **(G)** Boxplots of percentage of
1097 HMEC-1 infected with Δ*actA* Lm (actAp::mTagRFP) for cells residing on soft (3 kPa) or stiff (70
1098 kPa) hydrogels and pre-treated for 2 h either with vehicle control or 100 nM Angiotensin-II (N=6
1099 replicates). MOI is 62.5. Two asterisks denote statistically significant differences between the
1100 medians of two distributions (<0.01; Wilcoxon rank sum test).
1101
1102 **Figure S3. Met-dependent decrease in bacterial uptake.** (**A)** Western blot from whole HMEC-
1103 1 lysates showing expression of Met for cells seeded on soft (3 kPa), stiff (70 kPa) and TC
1104 polystyrene substrates treated or not with 2 μM PF537228 FAK inhibitor. In each case, equal
1105 quantities of protein were loaded and equal loading was also confirmed in relation to
1106 glyceraldehyde 3-phosphate dehydrogenase (GAPDH) expression. (**B-C)** Histograms of the
1107 logarithm of Lm fluorescence intensity per cell for HMEC-1 treated with 20 nM of non-targeting
1108 siRNA (siNT) **(C)** or Met siRNA (siMet) **(D)**. HMEC-1 were infected with *ΔactA* Lm
1109 (actAp::mTagRFP) and infection was analyzed by flow cytometry, 7–8 h after infection. MOI is
1110 45. Histograms for N=6 replicates are shown in different colors. Control uninfected cells'
1111 histogram is shown in purple. Based on the autofluorescence of the control group a gate is
1112 defined (see black and red lines) showing what is considered uninfected (left, black line) and
1113 infected (right, red line). **(D)** Relative with respect to GAPDH gene expression of Met obtained
1114 by RT-qPCR. The levels relative levels of expression in each siRNA treated sample (#1-#3) are
1115 expressed relative to the control siNT treated sample #2 (normalized relative quantity, NRQ).
1116 N=3 replicates are shown for each group treated with either siNT or siVIM. **(E)** Boxplots of
1117 percentage of HMEC-1 infected with Δ*actA*/Δ*inlB* Lm (actAp::mTagRFP) for cells HMEC-1
1118 treated with siNT or siMet (N=4 replicates). MOI is 60.
1119
1120 **Figure S4. Knocking down vimentin decreases Lm uptake. (A)** HMEC-1 treated with 20 nM
1121 of non-targeting siRNA (siNT, first row**)** or VIM siRNA (siVIM, second row**)** were stained for VIM

using the H-84 anti-vimentin antibody. Representative phase image of cells (Phase, left column), superimposed with the image of the nuclei (blue) and anti-vimentin antibody fluorescence (green, right column) are shown. Scale bar shown in white is 35 μm. **(B)** Relative with respect to GAPDH gene expression of vimentin obtained by RT-qPCR. The levels relative levels of expression in each siRNA treated sample (#1-#3) are expressed relative to the control siNT treated sample #2 (normalized relative quantity, NRQ). N=3 replicates are shown for each group treated with either siNT or siVIM (**C-D)** Histograms of the logarithm of Lm fluorescence intensity per cell for HMEC-1 treated with 20 nM of non-targeting siRNA (siNT) **(C)** or vimentin siRNA (siVIM) **(D)**. HMEC-1 were infected with *ΔactA* Lm (actAp::mTagRFP) and infection was analyzed by flow cytometry, 7–8 h after infection. MOI is 34. Histograms for N=6 replicates are shown in different colors. Control uninfected cells' histogram is shown in purple. Based on the autofluorescence of the control group a gate is defined (see black and red lines) showing what is considered uninfected (left, black line) and infected (right, red line). **(E)** Number of HMEC-1 passed through the flow cell in 20 s, for N = 4 samples coming from wells treated with either siNT or siVIM. **(F)** Boxplots of percentage of HMEC-1 infected with *ΔactA* Lm for the data shown in panels C-D. One or two asterisks denote statistically significant differences between the medians of two distributions (<0.05 or <0.01, respectively; Wilcoxon rank sum test). (**F)** HMEC-1 residing on collagen I-coated glass substrates, treated with siNT or siVIM were also blocked for 1 h with anti-vimentin antibodies prior to infection. Cells were infected with Lm (constitutively expressing GFP) at an MOI of 1.25. 30 min post-infection samples were fixed, immunostained and infection was analyzed by microscopy followed by image processing. Boxplots shows total bacteria per cell for an average of N=650 cells analyzed per condition (**F)** HMEC-1 residing on collagen I-coated glass substrates, treated with siNT or siVIM were also treated for 30 min with vehicle control or 5 μM withaferin prior to infection. Cells were infected with Lm (constitutively expressing GFP) at an MOI of 1.25. 30 min post-infection samples were fixed, immunostained and infection was analyzed by microscopy followed by image processing. Boxplots shows total

1148 bacteria per cell for an average of N=630 cells analyzed per condition.

1149

1150 **Figure S5. Fewer Lm localize at cell-cell junctions for siVIM treated HMEC-1. (A-B)** HMEC-
1151 1 treated with 20 nM of non-targeting siRNA (siNT, A**)** or vimentin siRNA (siVIM, B**)** were
1152 infected with Lm at an MOI of 3. 30 min post-infection samples were fixed, stained for VE-
1153 cadherin that localizes all throughout the cell-cell junctions using an anti-VE-cadherin antibody.
1154 Representative phase image of cells (left column), superimposed with the image of the nuclei
1155 (blue) and anti-VE-cadherin antibody fluorescence (white, right column) superimposed with
1156 fluorescence of Lm (red). Scale bar is 23 μm. Two representative examples are shown for each
1157 condition. Yellow arrows point at cell-cell junctions were bacteria are co-localized.

1158

1159 **SUPPLEMENTARY TABLES**

1160 **Supplementary Table 1. Bacterial strains used in this study.**

1161 **Supplementary Table 2. Synthetic siRNA pools used in this study.**

1162

REFERENCES

Acerbi, I., L. Cassereau, I. Dean, Q. Shi, A. Au, C. Park, Y.Y. Chen, J. Liphardt, E.S. Hwang, and V.M. Weaver. 2015. Human Breast Cancer Invasion and Aggression Correlates with ECM Stiffening and Immune Cell Infiltration. *Integrative biology : quantitative biosciences from nano to macro*. 7:1120-1134.

Ahmed, E.M. 2015. Hydrogel: Preparation, characterization, and applications: A review. *Journal of Advanced Research*. 6:105-121.

Aird, W.C. 2007. Phenotypic heterogeneity of the endothelium: I. Structure, function, and mechanisms. *Circ Res*. 100:158-173.

Aird, W.C. 2012. Endothelial Cell Heterogeneity. *Cold Spring Harbor Perspectives in Medicine*. 2.

Bargagna-Mohan, P., S.P. Deokule, K. Thompson, J. Wizeman, C. Srinivasan, S. Vooturi, U.B. Kompella, and R. Mohan. 2013. Withaferin A Effectively Targets Soluble Vimentin in the Glaucoma Filtration Surgical Model of Fibrosis. *PLOS ONE*. 8:e63881.

Bargagna-Mohan, P., A. Hamza, Y.-e. Kim, Y. Khuan Ho, N. Mor-Vaknin, N. Wendschlag, J. Liu, R.M. Evans, D.M. Markovitz, C.-G. Zhan, K.B. Kim, and R. Mohan. The Tumor Inhibitor and Antiangiogenic Agent Withaferin A Targets the Intermediate Filament Protein Vimentin. *Chemistry & Biology*. 14:623-634.

Bastounis, E., R. Meili, B. Alonso-Latorre, J. del Álamo, J. Lasheras, and R. Firtel. 2011. The SCAR/WAVE complex is necessary for proper regulation of traction stresses during amoeboid motility. *Mol Biol Cell*. 21:3995–4003.

Bastounis, E., R. Meili, B. Álvarez-González, J. Francois, J.C. del Álamo, R.A. Firtel, and J.C. Lasheras. 2014. Both contractile axial and lateral traction force dynamics drive amoeboid cell motility. *The Journal of Cell Biology*. 204:1045-1061.

Bhattacharya, R., A.M. Gonzalez, P.J. DeBiase, H.E. Trejo, R.D. Goldman, F.W. Flitney, and J.C.R. Jones. 2009. Recruitment of vimentin to the cell surface by β3 integrin and plectin mediates adhesion strength. *Journal of Cell Science*. 122:1390.

Bierne, H., and P. Cossart. 2002. InlB, a surface protein of *Listeria monocytogenes* that behaves as an invasin and a growth factor. *Journal of Cell Science*. 115:3357.

Birukova, A.A., X. Tian, I. Cokic, Y. Beckham, M. Gardel, and K.G. Birukov. 2013. Endothelial barrier disruption and recovery is controlled by substrate stiffness. *Microvascular research*. 87:50-57.

Blacher, J., R. Asmar, S. Djane, G.M. London, and M.E. Safar. 1999. Aortic pulse wave velocity as a marker of cardiovascular risk in hypertensive patients. *Hypertension*. 33:1111-1117.

Boutouyrie, P., A.I. Tropeano, R. Asmar, I. Gautier, A. Benetos, P. Lacolley, and S. Laurent. 2002. Aortic stiffness is an independent predictor of primary coronary events in hypertensive patients: a longitudinal study. *Hypertension*. 39:10-15.

Brundage, R.A., G.A. Smith, A. Camilli, J.A. Theriot, and D.A. Portnoy. 1993. Expression and phosphorylation of the Listeria monocytogenes ActA protein in mammalian cells. *Proceedings of the National Academy of Sciences of the United States of America*. 90:11890-11894.

Buchanan, S.G., J. Hendle, P.S. Lee, C.R. Smith, P.Y. Bounaud, K.A. Jessen, C.M. Tang, N.H. Huser, J.D. Felce, K.J. Froning, M.C. Peterman, B.E. Aubol, S.F. Gessert, J.M. Sauder, K.D. Schwinn, M. Russell, I.A. Rooney, J. Adams, B.C. Leon, T.H. Do, J.M. Blaney, P.A. Sprengeler, D.A. Thompson, L. Smyth, L.A. Pelletier, S. Atwell, K. Holme, S.R. Wasserman, S. Emtage, S.K. Burley, and S.H. Reich. 2009. SGX523 is an exquisitely selective, ATP-competitive inhibitor of the MET receptor tyrosine kinase with antitumor activity in vivo. *Mol Cancer Ther*. 8:3181-3190.

Burgess-Cassler, A., J.J. Johansen, D.A. Santek, J.R. Ide, and N.C. Kendrick. 1989. Computerized quantitative analysis of coomassie-blue-stained serum proteins separated by two-dimensional electrophoresis. *Clinical chemistry*. 35:2297-2304.

Chi, F., T.D. Jong, L. Wang, Y. Ouyang, C. Wu, W. Li, and S.H. Huang. 2010. Vimentin-mediated signalling is required for IbeA+ E. coli K1 invasion of human brain microvascular endothelial cells. *Biochem J*. 427:79-90.

Chien, S., S. Li, Y.T. Shiu, and Y.S. Li. 2005. Molecular basis of mechanical modulation of endothelial cell migration. *Front Biosci*. 10:1985-2000.

Claes, J., T. Vanassche, M. Peetermans, L. Liesenborghs, C. Vandenbriele, K. Vanhoorelbeke, D. Missiakas, O. Schneewind, M.F. Hoylaerts, R. Heying, and P. Verhamme. 2014. Adhesion of Staphylococcus aureus to the vessel wall under flow is mediated by von Willebrand factor-binding protein. *Blood*. 124:1669-1676.

Clarke, E.J., and V. Allan. 2002. Intermediate filaments: vimentin moves in. *Curr Biol*. 12.

Collins, C., L.D. Osborne, C. Guilluy, Z. Chen, E.T. O'Brien, J.S. Reader, K. Burridge, R. Superfine, and E. Tzima. 2014. Haemodynamic and extracellular matrix cues regulate the mechanical phenotype and stiffness of aortic endothelial cells. *Nature Communications*. 5:3984.

Craig, L.E., J.P. Spelman, J.D. Strandberg, and M.C. Zink. 1998. Endothelial Cells from Diverse Tissues Exhibit Differences in Growth and Morphology. *Microvascular Research*. 55:65-76.

Darie, C.C., K. Deinhardt, G. Zhang, H.S. Cardasis, M.V. Chao, and T.A. Neubert. 2011. Identifying transient protein-protein interactions in EphB2 signaling by blue native PAGE and mass spectrometry. *Proteomics*. 11:4514-4528.

Das, S., V. Ravi, and A. Desai. 2011. Japanese encephalitis virus interacts with vimentin to facilitate its entry into porcine kidney cell line. *Virus Res*. 160.

Discher, D.E., P.A. Janmey, and Y.L. Wang. 2005. Tissue cells feel and respond to the stiffness of their substrate. *Science*. 310:1139-1143.

Drevets, D.A., R.T. Sawyer, T.A. Potter, and P.A. Campbell. 1995. Listeria monocytogenes infects human endothelial cells by two distinct mechanisms. *Infect Immun*. 63:4268-4276.

Du, J., Y. Zu, J. Li, S. Du, Y. Xu, L. Zhang, L. Jiang, Z. Wang, S. Chien, and C. Yang. 2016. Extracellular matrix stiffness dictates Wnt expression through integrin pathway. *Scientific Reports*. 6:20395.

Du, N., H. Cong, H. Tian, H. Zhang, W. Zhang, L. Song, and P. Tien. 2014. Cell Surface Vimentin Is an Attachment Receptor for Enterovirus 71. *Journal of Virology*. 88:5816-5833.

Dussurget, O., J. Pizarro-Cerda, and P. Cossart. 2004. Molecular determinants of Listeria monocytogenes virulence. *Annu Rev Microbiol*. 58:587-610.

Edelstein, A.D., M.A. Tsuchida, N. Amodaj, H. Pinkard, R.D. Vale, and N. Stuurman. 2014. Advanced methods of microscope control using μManager software. *Journal of Biological Methods; Vol 1, No 2 (2014)*.

Elia, G. 2012. Cell surface protein biotinylation for SDS-PAGE analysis. *Methods Mol Biol*. 869:361-372.

Fiedler, F. 1988. Biochemistry of the cell surface of Listeria strains: a locating general view. *Infection*. 16 Suppl 2:S92-97.

Fuchs, E., and K. Weber. 1994. Intermediate filaments: structure, dynamics, function, and disease. *Annu Rev Biochem*. 63:345-382.

Fujimoto, T., S. Nakade, A. Miyawaki, K. Mikoshiba, and K. Ogawa. 1992. Localization of inositol 1,4,5-trisphosphate receptor-like protein in plasmalemmal caveolae. *J Cell Biol*. 119:1507-1513.

Garg, A., P.F. Barnes, A. Porgador, S. Roy, S. Wu, J.S. Nanda, D.E. Griffith, W.M. Girard, N. Rawal, S. Shetty, and R. Vankayalapati. 2006. Vimentin expressed on Mycobacterium tuberculosis-infected human monocytes is involved in binding to the NKp46 receptor. *J Immunol*. 177:6192-6198.

Gattazzo, F., A. Urciuolo, and P. Bonaldo. 2014. Extracellular matrix: A dynamic microenvironment for stem cell niche. *Biochimica et Biophysica Acta*. 1840:2506-2519.
Geiger, B., J.P. Spatz, and A.D. Bershadsky. 2009. Environmental sensing through focal adhesions. *Nat Rev Mol Cell Biol*. 10:21-33.
Georges, P., W. Miller, D. Meaney, E. Sawyer, and P.A. Janmey. 2006. Matrices with compliance comparable to that of brain tissue select neuronal over glial growth in mixed cortical cultures. *Biophys J*. 90:3012-3018.
Glaser, P., L. Frangeul, C. Buchrieser, C. Rusniok, A. Amend, F. Baquero, P. Berche, H. Bloecker, P. Brandt, T. Chakraborty, A. Charbit, F. Chetouani, E. Couve, A. de Daruvar, P. Dehoux, E. Domann, G. Dominguez-Bernal, E. Duchaud, L. Durant, O. Dussurget, K.D. Entian, H. Fsihi, F. Garcia-del Portillo, P. Garrido, L. Gautier, W. Goebel, N. Gomez-Lopez, T. Hain, J. Hauf, D. Jackson, L.M. Jones, U. Kaerst, J. Kreft, M. Kuhn, F. Kunst, G. Kurapkat, E. Madueno, A. Maitournam, J.M. Vicente, E. Ng, H. Nedjari, G. Nordsiek, S. Novella, B. de Pablos, J.C. Perez-Diaz, R. Purcell, B. Remmel, M. Rose, T. Schlueter, N. Simoes, A. Tierrez, J.A. Vazquez-Boland, H. Voss, J. Wehland, and P. Cossart. 2001. Comparative genomics of Listeria species. *Science*. 294:849-852.
Gopal, S., A. Bober, J.R. Whiteford, H.A. Multhaupt, A. Yoneda, and J.R. Couchman. 2010. Heparan sulfate chain valency controls syndecan-4 function in cell adhesion. *J Biol Chem*. 285:14247-14258.
Greco, S., M.G. Elia, A. Muscella, C. Storelli, and S. Marsigliante. 2002. AT1 Angiotensin II receptor mediates intracellular calcium mobilization in normal and cancerous breast cells in primary culture. *Cell calcium*. 32:1-10.
Greiffenberg, L., W. Goebel, K.S. Kim, I. Weiglein, A. Bubert, F. Engelbrecht, M. Stins, and M. Kuhn. 1998. Interaction of Listeria monocytogenes with human brain microvascular endothelial cells: InlB-dependent invasion, long-term intracellular growth, and spread from macrophages to endothelial cells. *Infect Immun*. 66:5260-5267.
Greiffenberg, L., Z. Sokolovic, H.-J. Schnittler, A. Spory, R. Böckmann, W. Goebel, and M. Kuhn. 1997. Listeria monocytogenes-infected human umbilical vein endothelial cells: internalin-independent invasion, intracellular growth, movement, and host cell responses. *FEMS Microbiology Letters*. 157:163-170.
Gundelfinger, E.D., M.M. Kessels, and B. Qualmann. 2003. Temporal and spatial coordination of exocytosis and endocytosis. *Nature Rev. Mol. Cell Biol.* 4:127-139.
Henry-Stanley, M.J., D.J. Hess, E.A. Erickson, R.M. Garni, and C.L. Wells. 2003. Role of heparan sulfate in interactions of Listeria monocytogenes with enterocytes. *Medical Microbiology and Immunology*. 192:107-115.
Higuita-Castro, N., C. Mihai, D.J. Hansford, and S.N. Ghadiali. 2014. Influence of airway wall compliance on epithelial cell injury and adhesion during interfacial flows. *Journal of Applied Physiology*. 117:1231-1242.
Huang, C., P.J. Butler, S. Tong, H.S. Muddana, G. Bao, and S. Zhang. 2013. Substrate stiffness regulates cellular uptake of nanoparticles. *Nano letters*. 13:1611-1615.
Huynh, J., N. Nishimura, K. Rana, J.M. Peloquin, J.P. Califano, C.R. Montague, M.R. King, C.B. Schaffer, and C.A. Reinhart-King. 2011. Age-related intimal stiffening enhances endothelial permeability and leukocyte transmigration. *Sci Transl Med*. 3:112-122.
Ingram, D.A., L.E. Mead, H. Tanaka, V. Meade, A. Fenoglio, K. Mortell, K. Pollok, M.J. Ferkowicz, D. Gilley, and M.C. Yoder. 2004. Identification of a novel hierarchy of endothelial progenitor cells using human peripheral and umbilical cord blood. *Blood*. 104:2752-2760.
Ise, H., S. Kobayashi, M. Goto, T. Sato, M. Kawakubo, M. Takahashi, U. Ikeda, and T. Akaike. 2010. Vimentin and desmin possess GlcNAc-binding lectin-like properties on cell surfaces. *Glycobiology*. 20:843-864.
Jackson, K.A., M. Iwamoto, and D. Swerdlow. 2010. Pregnancy-associated listeriosis. *Epidemiol Infect*. 138:1503-1509.

Janmey, P.A., and R.T. Miller. 2011. Mechanisms of mechanical signaling in development and disease. *Journal of Cell Science*. 124:9-18.
Karhemo, P.-R., S. Ravela, M. Laakso, I. Ritamo, O. Tatti, S. Mäkinen, S. Goodison, U.-H. Stenman, E. Hölttä, S. Hautaniemi, L. Valmu, K. Lehti, and P. Laakkonen. 2012. An optimized isolation of biotinylated cell surface proteins reveals novel players in cancer metastasis. *Journal of proteomics*. 77:87-100.
Khatiwala, C.B., S.R. Peyton, and A.J. Putnam. 2006. Intrinsic mechanical properties of the extracellular matrix affect the behavior of pre-osteoblastic MC3T3-E1 cells. *American Journal of Physiology - Cell Physiology*. 290:C1640.
Kirchner, M., and D.E. Higgins. 2008. Inhibition of ROCK activity allows InlF-mediated invasion and increased virulence of Listeria monocytogenes. *Mol Microbiol*. 68:749-767.
Klein, E.A., L. Yin, D. Kothapalli, P. Castagnino, F.J. Byfield, T. Xu, I. Levental, E. Hawthorne, P.A. Janmey, and R.K. Assoian. 2009. Cell-cycle control by physiological matrix elasticity and in vivo tissue stiffening. *Curr Biol*. 19:1511-1518.
Kocks, C., E. Gouin, M. Tabouret, P. Berche, H. Ohayon, and P. Cossart. 1992. L. monocytogenes-induced actin assembly requires the actA gene product, a surface protein. *Cell*. 68:521-531.
Kohn, Julie C., Dennis W. Zhou, F. Bordeleau, Allen L. Zhou, Brooke N. Mason, Michael J. Mitchell, Michael R. King, and Cynthia A. Reinhart-King. 2015. Cooperative Effects of Matrix Stiffness and Fluid Shear Stress on Endothelial Cell Behavior. *Biophysical Journal*. 108:471-478.
Kolewe, K.W., S.R. Peyton, and J.D. Schiffman. 2015. Fewer Bacteria Adhere to Softer Hydrogels. *ACS Appl Mater Interfaces*. 7:19562-19569.
Konopka, J.B. 2012. N-acetylglucosamine (GlcNAc) functions in cell signaling. *Scientifica*. 2012.
Kothapalli, D., S.-L. Liu, Y.H. Bae, J. Monslow, T. Xu, E.A. Hawthorne, F.J. Byfield, P. Castagnino, S. Rao, D.J. Rader, E. Puré, M.C. Phillips, S. Lund-Katz, P.A. Janmey, and R.K. Assoian. 2012. Cardiovascular protection by apoE and apoE-HDL linked to suppression of ECM gene expression and arterial stiffening. *Cell reports*. 2:1259-1271.
Koudelka, K.J., G. Destito, E.M. Plummer, S.A. Trauger, G. Siuzdak, and M. Manchester. 2009. Endothelial targeting of cowpea mosaic virus (CPMV) via surface vimentin. *PLoS Pathog*. 5.
Krishnan, R., D.D. Klumpers, C.Y. Park, K. Rajendran, X. Trepat, J. van Bezu, V.W.M. van Hinsbergh, C.V. Carman, J.D. Brain, J.J. Fredberg, J.P. Butler, and G.P. van Nieuw Amerongen. 2011. Substrate stiffening promotes endothelial monolayer disruption through enhanced physical forces. *American Journal of Physiology - Cell Physiology*. 300:C146-C154.
Lauer, P., M.Y. Chow, M.J. Loessner, D.A. Portnoy, and R. Calendar. 2002. Construction, characterization, and use of two Listeria monocytogenes site-specific phage integration vectors. *Journal of bacteriology*. 184:4177-4186.
Lebrun, M., J. Mengaud, H. Ohayon, F. Nato, and P. Cossart. 1996. Internalin must be on the bacterial surface to mediate entry of Listeria monocytogenes into epithelial cells. *Mol Microbiol*. 21:579-592.
Lecuit, M., R. Hurme, J. Pizarro-Cerda, H. Ohayon, B. Geiger, and P. Cossart. 2000. A role for alpha-and beta-catenins in bacterial uptake. *Proc Natl Acad Sci U S A*. 97:10008-10013.
Lemichez, E., M. Lecuit, X. Nassif, and S. Bourdoulous. 2010. Breaking the wall: targeting of the endothelium by pathogenic bacteria. *Nat Rev Micro*. 8:93-104.
Li, S., M. Kim, Y.L. Hu, S. Jalali, D.D. Schlaepfer, T. Hunter, S. Chien, and J.Y. Shyy. 1997. Fluid shear stress activation of focal adhesion kinase. Linking to mitogen-activated protein kinases. *J Biol Chem*. 272:30455-30462.
Liu, D., Z. Shriver, G. Venkataraman, Y. El Shabrawi, and R. Sasisekharan. 2002. Tumor cell surface heparan sulfate as cryptic promoters or inhibitors of tumor growth and metastasis. *Proceedings of the National Academy of Sciences*. 99:568-573.

Louis, H., A. Kakou, V. Regnault, C. Labat, A. Bressenot, J. Gao-Li, H. Gardner, S.N. Thornton, P. Challande, Z. Li, and P. Lacolley. 2007. Role of alpha1beta1-integrin in arterial stiffness and angiotensin-induced arterial wall hypertrophy in mice. *American journal of physiology. Heart and circulatory physiology*. 293:H2597-2604.

Mak, T.N., and H. Brüggemann. 2016. Vimentin in Bacterial Infections. *Cells*. 5:18.

Mathieu, S.V., K.S. Aragão, A. Imberty, and A. Varrot. 2010. Discoidin I from *Dictyostelium discoideum* and interactions with oligosaccharides: specificity, affinity, crystal structures and comparison with Discoidin II. *Journal of molecular biology*. 400:540-554.

Mengaud, J., H. Ohayon, P. Gounon, R.M. Mege, and P. Cossart. 1996. E-cadherin is the receptor for internalin, a surface protein required for entry of L. monocytogenes into epithelial cells. *Cell*. 84:923-932.

Mih, J.D., A.S. Sharif, F. Liu, A. Marinkovic, M.M. Symer, and D.J. Tschumperlin. 2011. A Multiwell Platform for Studying Stiffness-Dependent Cell Biology. *PLoS ONE*. 6:e19929.

Mitra, A., A. Satelli, X. Xia, J. Cutrera, L. Mishra, and S. Li. 2015. Cell-surface Vimentin: A mislocalized protein for isolating csVimentin(+) CD133(-) novel stem-like hepatocellular carcinoma cells expressing EMT markers. *International journal of cancer*. 137:491-496.

Montiel, M., E.P. de la Blanca, and E. Jimenez. 2005. Angiotensin II induces focal adhesion kinase/paxillin phosphorylation and cell migration in human umbilical vein endothelial cells. *Biochemical and biophysical research communications*. 327:971-978.

Mor-Vaknin, N., A. Punturieri, K. Sitwala, and D.M. Markovitz. 2003. Vimentin is secreted by activated macrophages. *Nat Cell Biol*. 5:59-63.

Niddam, A.F., R. Ebady, A. Bansal, A. Koehler, B. Hinz, and T.J. Moriarty. 2017. Plasma fibronectin stabilizes Borrelia burgdorferi-endothelial interactions under vascular shear stress by a catch-bond mechanism. *Proc Natl Acad Sci U S A*. 114:E3490-e3498.

Nunomura, K., K. Nagano, C. Itagaki, M. Taoka, N. Okamura, Y. Yamauchi, S. Sugano, N. Takahashi, T. Izumi, and T. Isobe. 2005. Cell surface labeling and mass spectrometry reveal diversity of cell surface markers and signaling molecules expressed in undifferentiated mouse embryonic stem cells. *Molecular & cellular proteomics : MCP*. 4:1968-1976.

O'Farrell, P.H. 1975. High resolution two-dimensional electrophoresis of proteins. *J Biol Chem*. 250:4007-4021.

Oakley, B.R., D.R. Kirsch, and N.R. Morris. 1980. A simplified ultrasensitive silver stain for detecting proteins in polyacrylamide gels. *Analytical biochemistry*. 105:361-363.

Onken, M.D., O.L. Mooren, S. Mukherjee, S.T. Shahan, J. Li, and J.A. Cooper. 2014. Endothelial Monolayers and Transendothelial Migration Depend on Mechanical Properties of the Substrate. *Cytoskeleton (Hoboken, N.J.)*. 71:695-706.

Ostrowski, Maggie A., Ngan F. Huang, Travis W. Walker, T. Verwijlen, C. Poplawski, Amanda S. Khoo, John P. Cooke, Gerald G. Fuller, and Alexander R. Dunn. 2014. Microvascular Endothelial Cells Migrate Upstream and Align Against the Shear Stress Field Created by Impinging Flow. *Biophysical Journal*. 106:366-374.

Päll, T., A. Pink, L. Kasak, M. Turkina, W. Anderson, A. Valkna, and P. Kogerman. 2011. Soluble CD44 Interacts with Intermediate Filament Protein Vimentin on Endothelial Cell Surface. *PLOS ONE*. 6:e29305.

Parida, S.K., E. Domann, M. Rohde, S. Muller, A. Darji, T. Hain, J. Wehland, and T. Chakraborty. 1998. Internalin B is essential for adhesion and mediates the invasion of Listeria monocytogenes into human endothelial cells. *Mol Microbiol*. 28:81-93.

Pelham, R.J., and Y.I. Wang. 1997. Cell locomotion and focal adhesions are regulated by substrate flexibility. *Proc Natl Acad Sci U S A*. 94:13661.

Pizarro-Cerdá, J., and P. Cossart. 2006. Bacterial Adhesion and Entry into Host Cells. *Cell*. 124:715-727.

Provenzano, P.P., D.R. Inman, K.W. Eliceiri, and P.J. Keely. 2009. Matrix density-induced mechanoregulation of breast cell phenotype, signaling, and gene expression through a FAK-ERK linkage. *Oncogene*. 28:4326-4343.
Reed, S.C., R.L. Lamason, V.I. Risca, E. Abernathy, and M.D. Welch. 2014. Rickettsia actin-based motility occurs in distinct phases mediated by different actin nucleators. *Curr Biol*. 24:98-103.
Reinhart-King, C.A. 2008. Endothelial cell adhesion and migration. *Methods Enzymol*. 443:45-64.
Rengarajan, M., A. Hayer, and J.A. Theriot. 2016. Endothelial Cells Use a Formin-Dependent Phagocytosis-Like Process to Internalize the Bacterium Listeria monocytogenes. *PLoS Pathog*. 12:e1005603.
Roesli, C., D. Mumprecht V Fau - Neri, M. Neri D Fau - Detmar, and M. Detmar. Identification of the surface-accessible, lineage-specific vascular proteome by two-dimensional peptide mapping.
Rohrbeck, A., A. Schroder, S. Hagemann, A. Pich, M. Holtje, G. Ahnert-Hilger, and I. Just. 2014. Vimentin mediates uptake of C3 exoenzyme. *PLoS One*. 9:e101071.
Schwartz, M.A. 2010. Integrins and Extracellular Matrix in Mechanotransduction. *Cold Spring Harbor Perspectives in Biology*. 2:a005066.
Selinummi, J., J. Seppala, O. Yli-Harja, and J.A. Puhakka. 2005. Software for quantification of labeled bacteria from digital microscope images by automated image analysis. *Biotechniques*. 39:859-863.
Senger, D.R., C.A. Perruzzi, M. Streit, V.E. Koteliansky, A.R. de Fougerolles, and M. Detmar. 2002. The α(1)β(1) and α(2)β(1) Integrins Provide Critical Support for Vascular Endothelial Growth Factor Signaling, Endothelial Cell Migration, and Tumor Angiogenesis. *The American Journal of Pathology*. 160:195-204.
Shen, Y., I. Kawamura, T. Nomura, K. Tsuchiya, H. Hara, and S.R. Dewamitta. 2010. TLR2-MyD88-dependent PI3K and Rac1 activation facilitates the phagocytosis of Listeria monocytogenes by murine macrophages. *Infect Immun*. 78.
Shevchenko, A., M. Wilm, O. Vorm, and M. Mann. 1996. Mass spectrometric sequencing of proteins silver-stained polyacrylamide gels. *Anal Chem*. 68:850-858.
Shi, Z.-D., and J.M. Tarbell. 2011. Fluid Flow Mechanotransduction in Vascular Smooth Muscle Cells and Fibroblasts. *Annals of biomedical engineering*. 39:1608-1619.
Shigyo, M., T. Kuboyama, Y. Sawai, M. Tada-Umezaki, and C. Tohda. 2015. Extracellular vimentin interacts with insulin-like growth factor 1 receptor to promote axonal growth. *Scientific Reports*. 5:12055.
Sokolowska, I., C. Dorobantu, A.G. Woods, A. Macovei, N. Branza-Nichita, and C.C. Darie. 2012a. Proteomic analysis of plasma membranes isolated from undifferentiated and differentiated HepaRG cells. *Proteome Sci*. 10:47.
Sokolowska, I., M.A. Gawinowicz, A.G. Ngounou Wetie, and C.C. Darie. 2012b. Disulfide proteomics for identification of extracellular or secreted proteins. *Electrophoresis*. 33:2527-2536.
Sokolowska, I., A.G. Woods, M.A. Gawinowicz, U. Roy, and C.C. Darie. 2012c. Identification of potential tumor differentiation factor (TDF) receptor from steroid-responsive and steroid-resistant breast cancer cells. *J Biol Chem*. 287:1719-1733.
Spellman, D.S., K. Deinhardt, C.C. Darie, M.V. Chao, and T.A. Neubert. 2008. Stable isotopic labeling by amino acids in cultured primary neurons: application to brain-derived neurotrophic factor-dependent phosphotyrosine-associated signaling. *Mol Cell Proteomics*. 7:1067-1076.
Sperling, L.H., and D.W. Friedman. 1969. Synthesis and mechanical behavior of interpenetrating polymer networks: Poly(ethyl acrylate) and polystyrene. *Journal of Polymer Science Part A-2: Polymer Physics*. 7:425-427.

Stroka, K.M., and H. Aranda-Espinoza. 2011. Endothelial cell substrate stiffness influences neutrophil transmigration via myosin light chain kinase-dependent cell contraction. *Blood*. 118:1632.

Tang, X., Q. Wen, T.B. Kuhlenschmidt, M.S. Kuhlenschmidt, P.A. Janmey, and T.A. Saif. 2012. Attenuation of Cell Mechanosensitivity in Colon Cancer Cells during In Vitro Metastasis. *PLoS ONE*. 7:e50443.

Torsoni, A.S., T.M. Marin, L.A. Velloso, and K.G. Franchini. 2005. RhoA/ROCK signaling is critical to FAK activation by cyclic stretch in cardiac myocytes. *American journal of physiology. Heart and circulatory physiology*. 289:H1488-1496.

Trepat, X., G. Lenormand, and J.J. Fredberg. 2008. Universality in cell mechanics. *Soft Matter*. 4:1750-1759.

Tse, J.R., and A.J. Engler. 2010. Preparation of hydrogel substrates with tunable mechanical properties. *Current protocols in cell biology*. Chapter 10:Unit 10.16.

Vazquez-Boland, J.A., M. Kuhn, P. Berche, T. Chakraborty, G. Dominguez-Bernal, W. Goebel, B. Gonzalez-Zorn, J. Wehland, and J. Kreft. 2001. Listeria pathogenesis and molecular virulence determinants. *Clin Microbiol Rev*. 14:584-640.

Vincent, L.G., Y.S. Choi, B. Alonso-Latorre, J.C. del Alamo, and A.J. Engler. 2013. Mesenchymal stem cell durotaxis depends on substrate stiffness gradient strength. *Biotechnology journal*. 8:472-484.

Volkman, B.F., K.E. Prehoda, J.A. Scott, F.C. Peterson, and W.A. Lim. 2002. Structure of the N-WASP EVH1 domain-WIP complex: insight into the molecular basis of Wiskott-Aldrich syndrome. *Cell*. 111:565-576.

Wells, R.G. 2008. The role of matrix stiffness in regulating cell behavior. *Hepatology*. 47:1394-1400.

Weng, Y.-I., and S.D. Shukla. 2002. Angiotensin II activation of focal adhesion kinase and pp60c-Src in relation to mitogen-activated protein kinases in hepatocytes. *Biochimica et Biophysica Acta (BBA) - Molecular Cell Research*. 1589:285-297.

Wilson, S.L., and D.A. Drevets. 1998. Listeria monocytogenes infection and activation of human brain microvascular endothelial cells. *J Infect Dis*. 178:1658-1666.

Wood, J.A., S.J. Liliensiek, P. Russell, P.F. Nealey, and C.J. Murphy. 2010. Biophysical Cueing and Vascular Endothelial Cell Behavior. *Materials*. 3.

Yam, P.T., and J.A. Theriot. 2004. Repeated cycles of rapid actin assembly and disassembly on epithelial cell phagosomes. *Mol Biol Cell*. 15:5647-5658.

Yang, J., L. Zou, Y. Yang, J. Yuan, Z. Hu, H. Liu, H. Peng, W. Shang, X. Zhang, J. Zhu, and X. Rao. 2016. Superficial vimentin mediates DENV-2 infection of vascular endothelial cells. *Scientific Reports*. 6:38372.

Ye, M., H.M. Sanchez, M. Hultz, Z. Yang, M. Bogorad, A.D. Wong, and P.C. Searson. 2014. Brain microvascular endothelial cells resist elongation due to curvature and shear stress. *Scientific Reports*. 4:4681.

Yeh, Y.-T., S.S. Hur, J. Chang, K.-C. Wang, J.-J. Chiu, Y.-S. Li, and S. Chien. 2012. Matrix Stiffness Regulates Endothelial Cell Proliferation through Septin 9. *PLoS ONE*. 7:e46889.

Yeung, T., P.C. Georges, L.A. Flanagan, B. Marg, M. Ortiz, M. Funaki, N. Zahir, W. Ming, V. Weaver, and P.A. Janmey. 2005. Effects of substrate stiffness on cell morphology, cytoskeletal structure, and adhesion. *Cell Motil Cytoskeleton*. 60:24-34.

Yu, Y.T.-C., S.-C. Chien, I.Y. Chen, C.-T. Lai, Y.-G. Tsay, S.C. Chang, and M.-F. Chang. 2016. Surface vimentin is critical for the cell entry of SARS-CoV. *Journal of Biomedical Science*. 23:14.

Zebda, N., O. Dubrovskyi, and K.G. Birukov. 2012. Focal adhesion kinase regulation of mechanotransduction and its impact on endothelial cell functions. *Microvascular research*. 83:71-81.

Zeldovich, V.B., J.R. Robbins, M. Kapidzic, P. Lauer, and A.I. Bakardjiev. 2011. Invasive extravillous trophoblasts restrict intracellular growth and spread of Listeria monocytogenes. *PLoS Pathog*. 7:e1002005.

Zieman, S.J., V. Melenovsky, and D.A. Kass. 2005. Mechanisms, pathophysiology, and therapy of arterial stiffness. *Arterioscler Thromb Vasc Biol*. 25:932-943.

Zou, Y., L. He, and S.H. Huang. 2006. Identification of a surface protein on human brain microvascular endothelial cells as vimentin interacting with Escherichia coli invasion protein IbeA. *Biochemical and biophysical research communications*. 351:625-630.

Figure 1

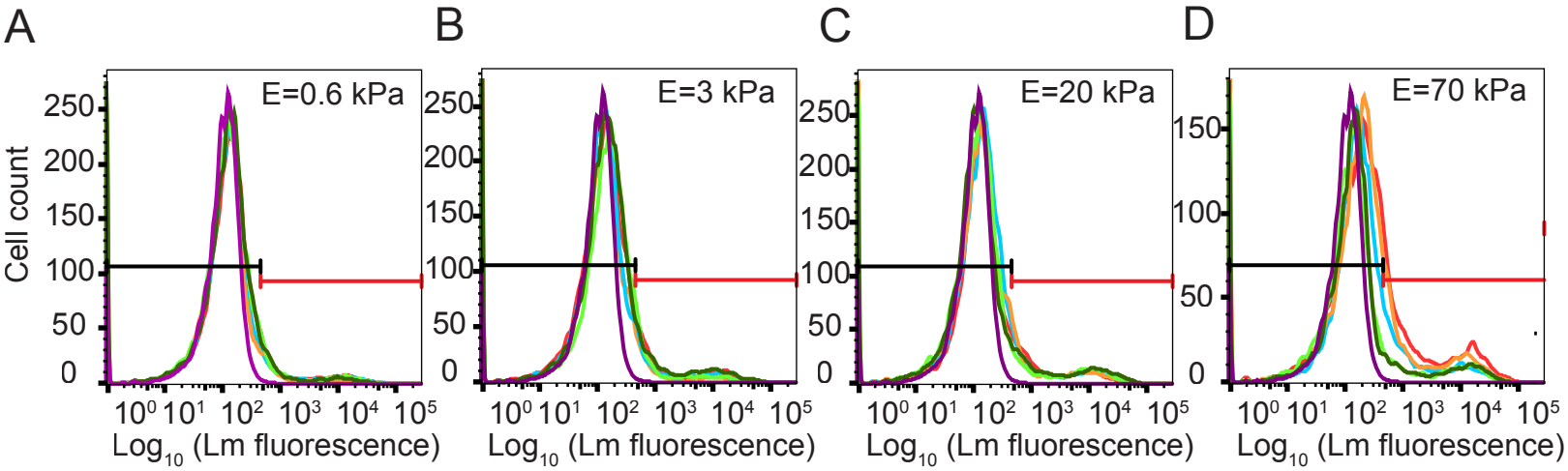
A
B
C
D
E=0.6 kPa
E=3 kPa
E=20 kPa
E=70 kPa
Cell count
Log10 (Lm fluorescence)

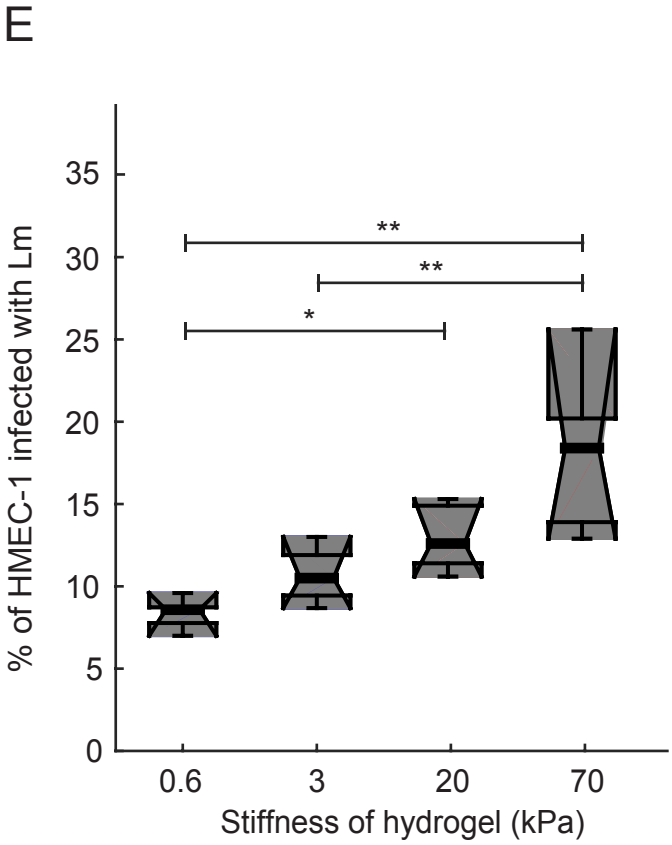
E
% of HMEC-1 infected with Lm
Stiffness of hydrogel (kPa)
0.6
3
20
70
**
**
*

Figure 2

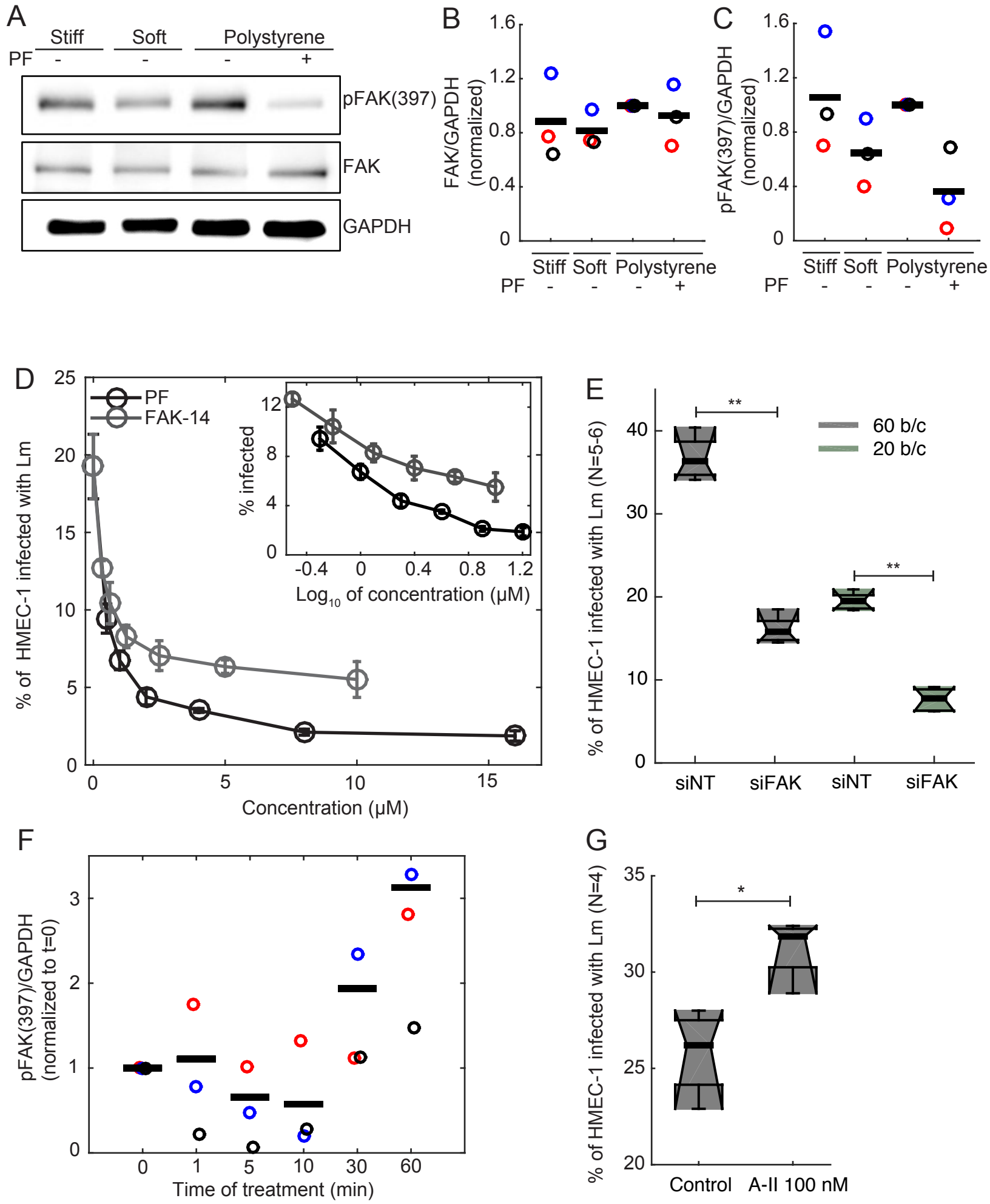
A
Stiff
Soft
Polystyrene
PF
-
-
-
+
pFAK(397)
FAK
GAPDH
B
FAK/GAPDH (normalized)
1.6
1.2
0.8
0.4
0
Stiff
Soft
Polystyrene
PF
-
-
-
+
C
pFAK(397)/GAPDH (normalized)
1.6
1.2
0.8
0.4
0
Stiff
Soft
Polystyrene
PF
-
-
-
+
D
PF
FAK-14
% of HMEC-1 infected with Lm
25
20
15
10
5
0
0
5
10
15
Concentration (μM)
% infected
12
8
4
0
-0.4
0
0.4
0.8
1.2
Log10 of concentration (μM)
E
% of HMEC-1 infected with Lm (N=5-6)
**
**
60 b/c
20 b/c
40
30
20
10
0
siNT
siFAK
siNT
siFAK
F
pFAK(397)/GAPDH (normalized to t=0)
3
2
1
0
0
1
5
10
30
60
Time of treatment (min)
G
% of HMEC-1 infected with Lm (N=4)
*
35
30
25
20
Control
A-II 100 nM

Figure 3

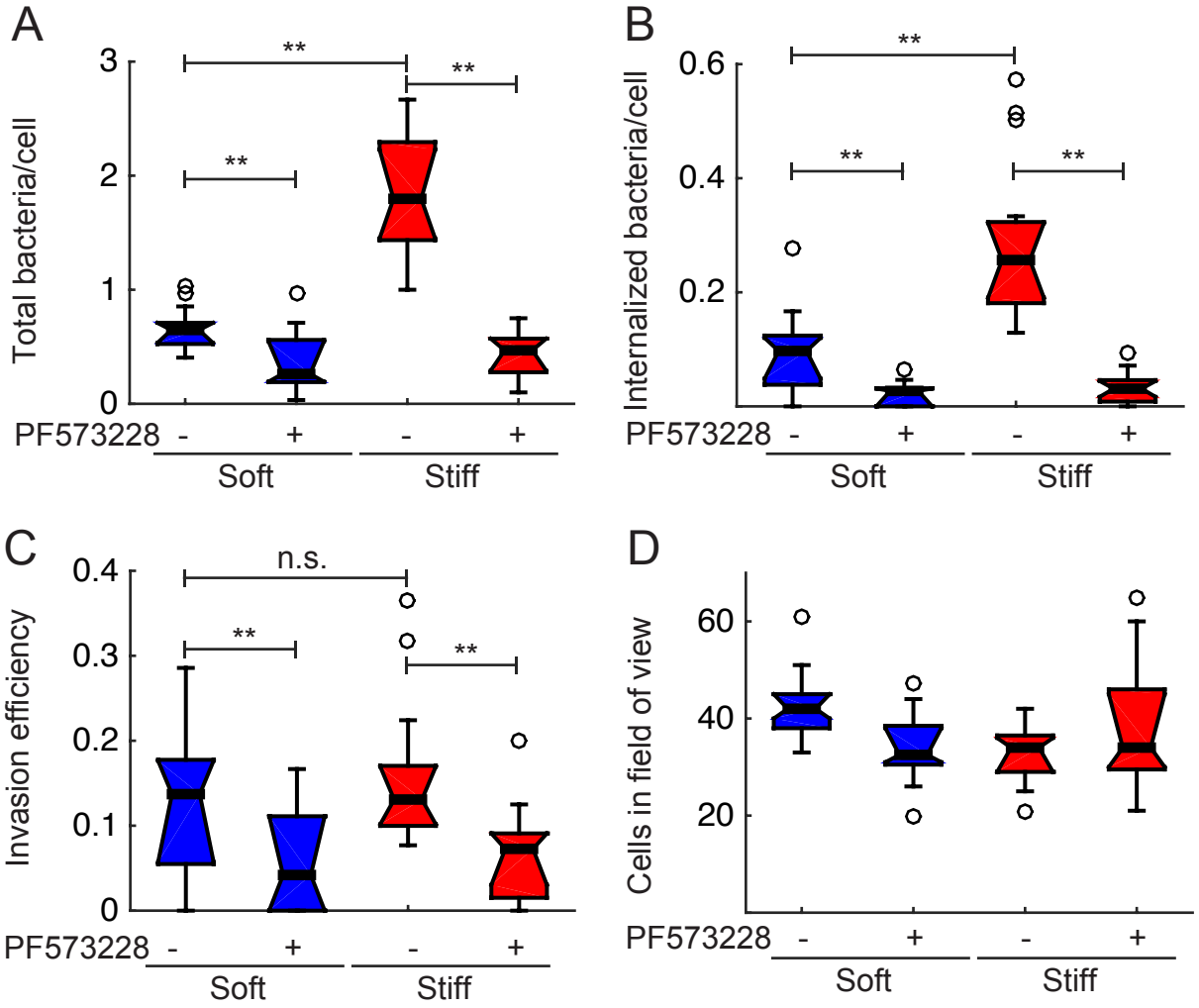
A
Total bacteria/cell
3
2
1
0
**
**
PF573228 - + - +
Soft
Stiff
B
Internalized bacteria/cell
0.6
0.4
0.2
**
**
**
PF573228 - + - +
Soft
Stiff
C
Invasion efficiency
0.4
0.3
0.2
0.1
0
n.s.
**
**
PF573228 - + - +
Soft
Stiff
D
Cells in field of view
60
40
20
PF573228 - + - +
Soft
Stiff

Figure 4

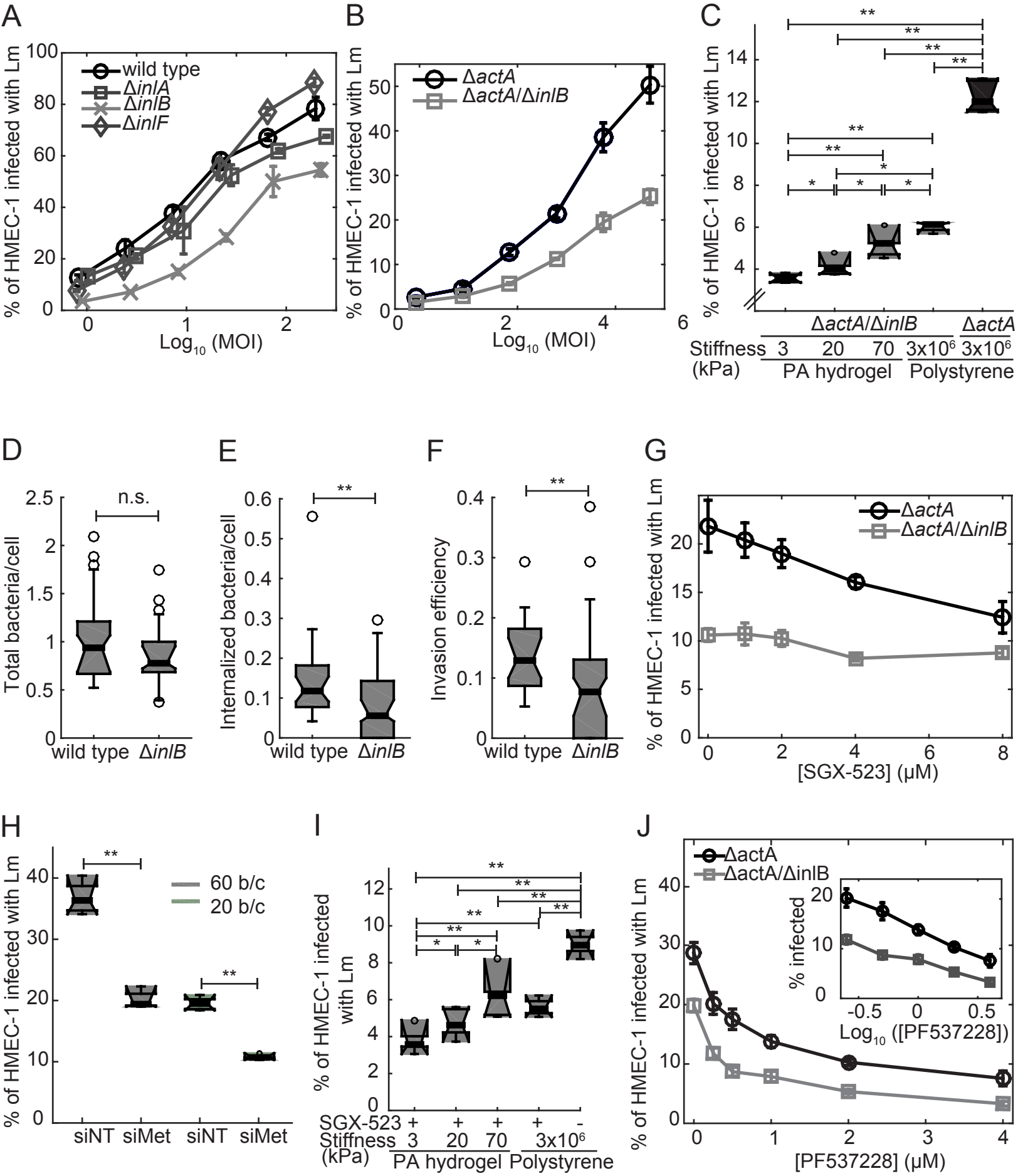
A
% of HMEC-1 infected with Lm
wild type
ΔinlA
ΔinlB
ΔinlF
Log10 (MOI)
B
ΔactA
ΔactA/ΔinlB
C
ΔactA/ΔinlB
ΔactA
Stiffness (kPa)
3
20
70
3x10^6
3x10^6
PA hydrogel
Polystyrene
D
Total bacteria/cell
n.s.
wild type
ΔinlB
E
Internalized bacteria/cell
F
Invasion efficiency
G
ΔactA
ΔactA/ΔinlB
[SGX-523] (μM)
H
60 b/c
20 b/c
siNT
siMet
I
SGX-523
J
ΔactA
ΔactA/ΔinlB
% infected
Log10 ([PF537228])
[PF537228] (μM)

Figure 5

A

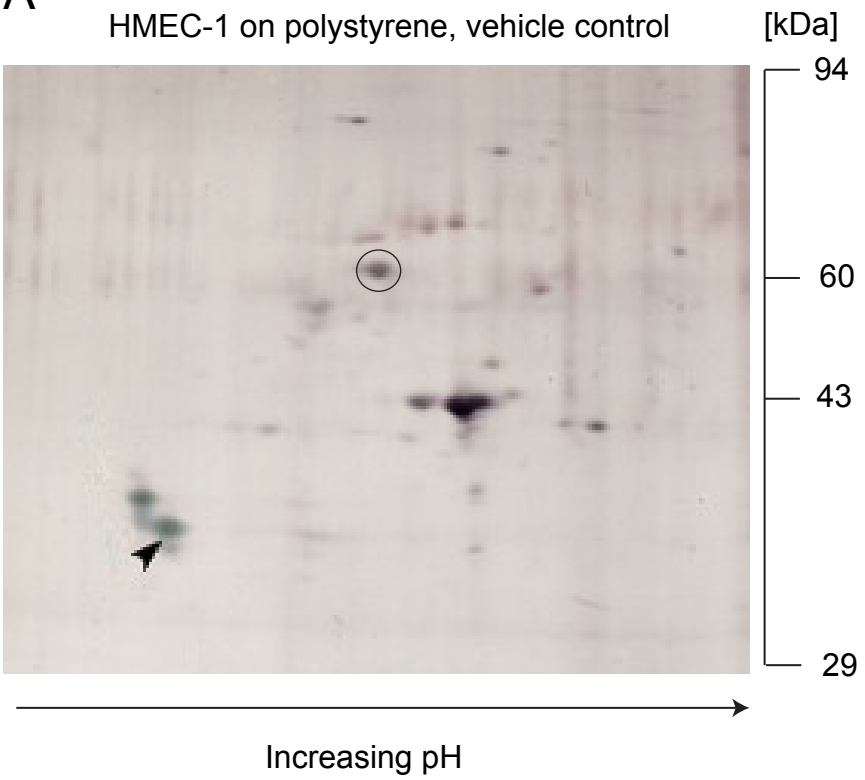
HMEC-1 on polystyrene, vehicle control
[kDa]
94
60
43
29
Increasing pH

B

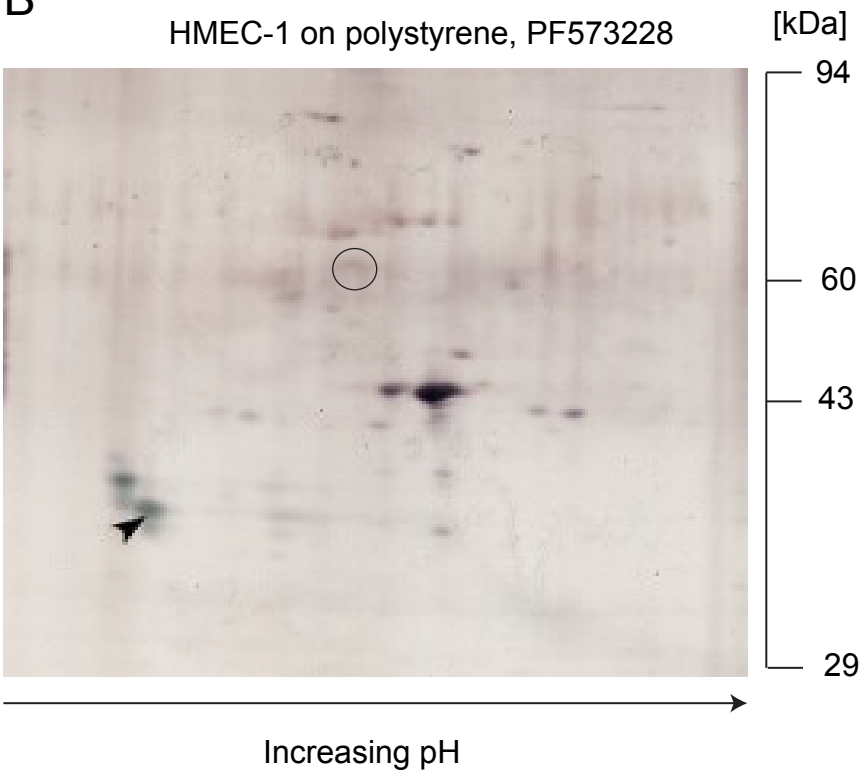
HMEC-1 on polystyrene, PF573228
[kDa]
94
60
43
29
Increasing pH

Figure 6

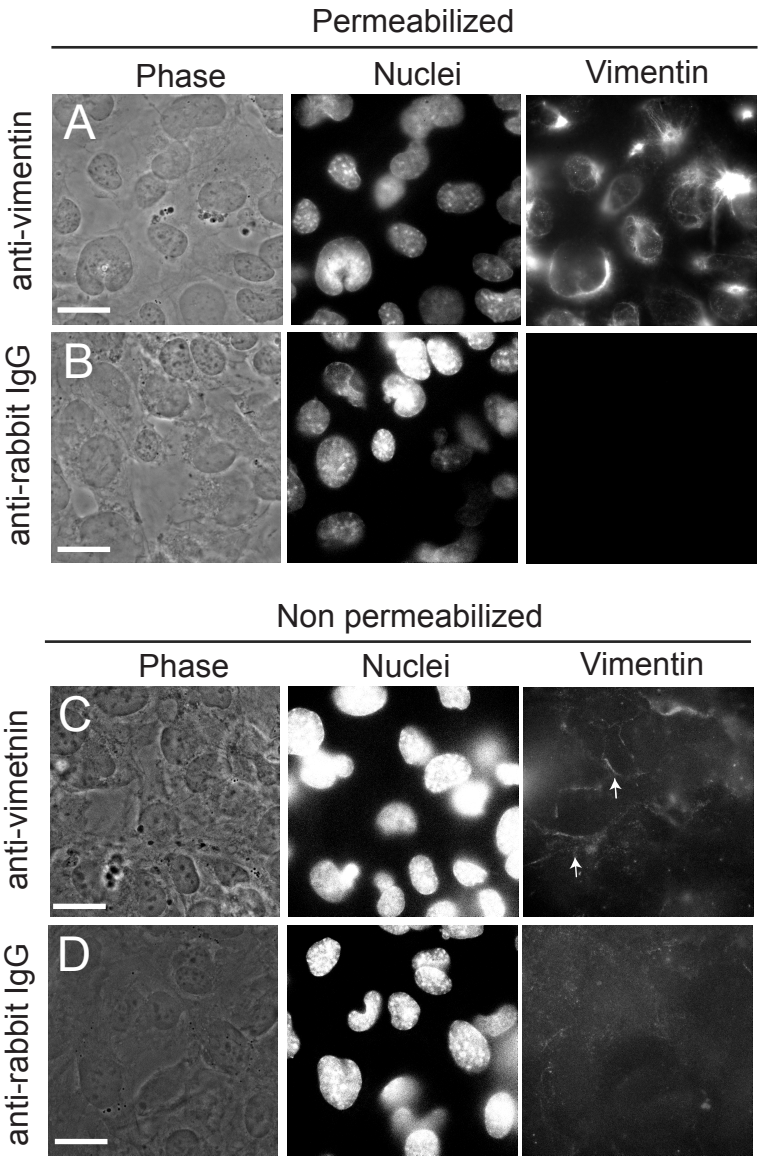
Permeabilized
Phase
Nuclei
Vimentin
anti-vimentin
A
anti-rabbit IgG
B
Non permeabilized
Phase
Nuclei
Vimentin
anti-vimetnin
C
anti-rabbit IgG
D

Figure 7

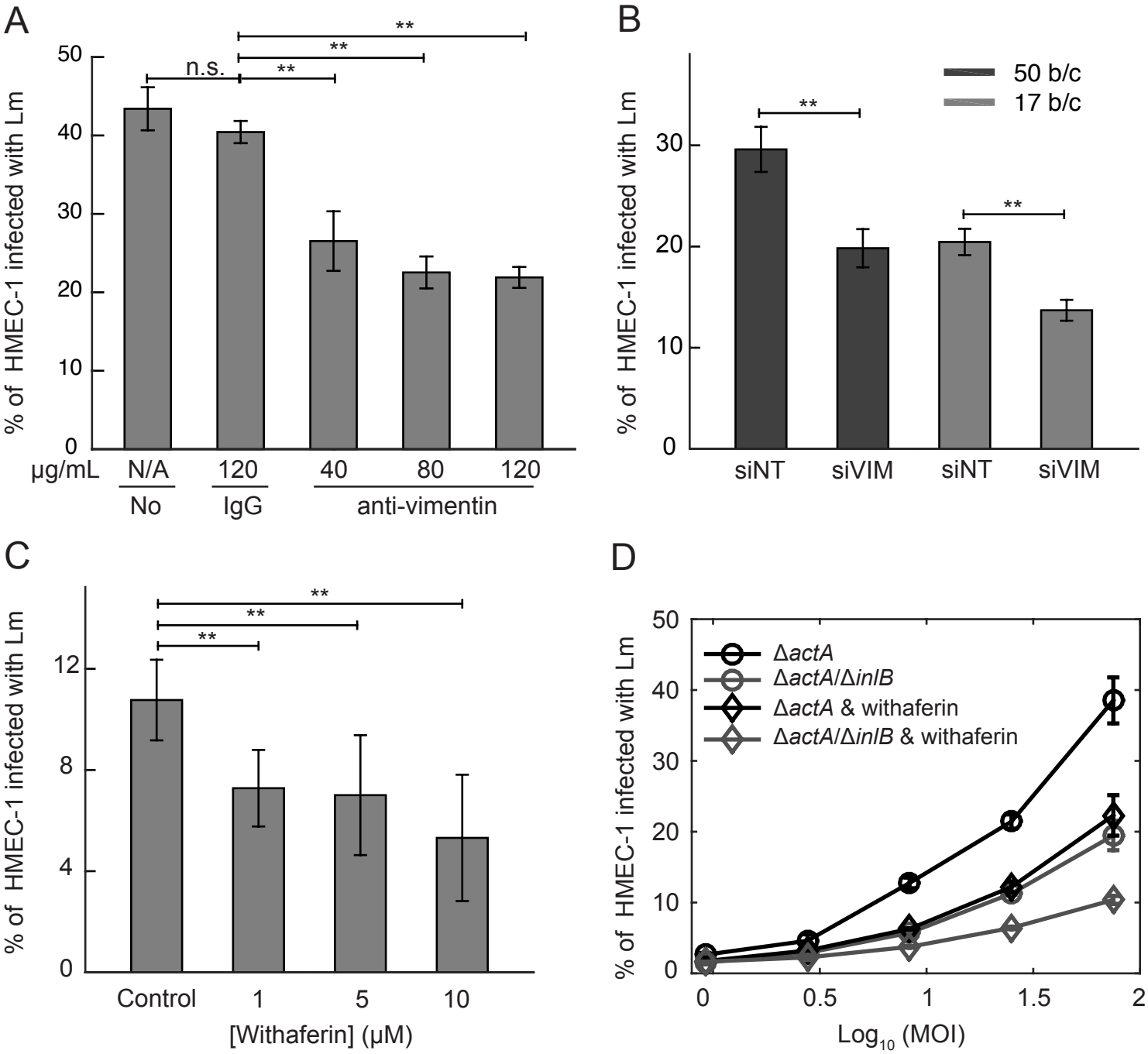
A
% of HMEC-1 infected with Lm
n.s.
**
**
**
μg/mL
N/A
120
40
80
120
No
IgG
anti-vimentin
B
50 b/c
17 b/c
**
**
siNT
siVIM
siNT
siVIM
C
**
**
**
Control
1
5
10
[Withaferin] (μM)
D
ΔactA
ΔactA/ΔinlB
ΔactA & withaferin
ΔactA/ΔinlB & withaferin
Log10 (MOI)

Figure 8

A

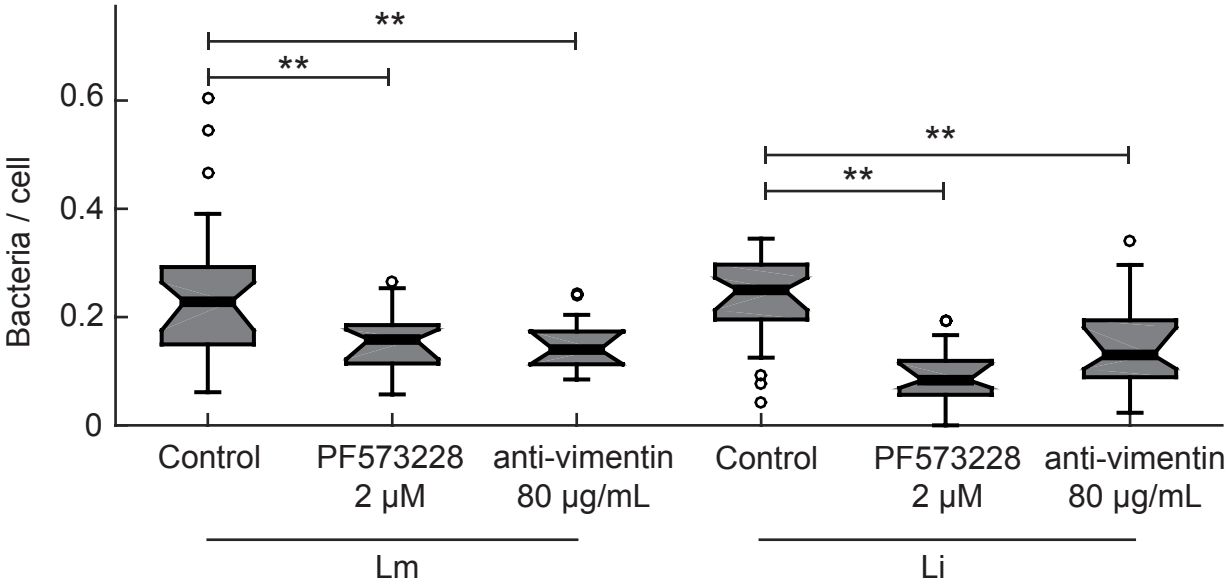
**
**
**
**
0.6
0.4
0.2
0
Bacteria / cell
Control
PF573228
2 μM
anti-vimentin
80 μg/mL
Control
PF573228
2 μM
anti-vimentin
80 μg/mL
Lm
Li

B

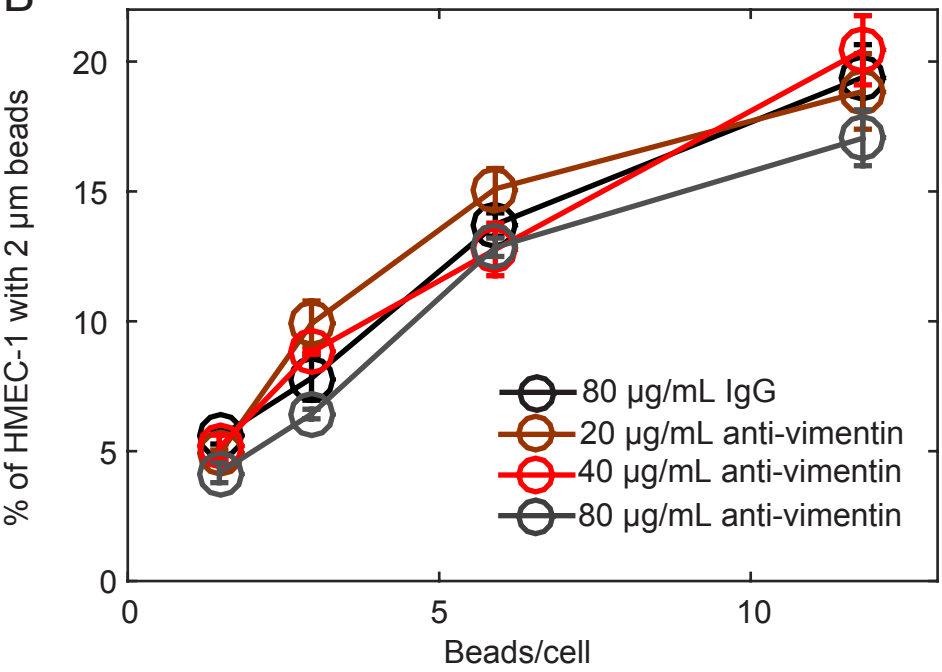
20
15
10
5
0
% of HMEC-1 with 2 μm beads
0
5
10
Beads/cell
80 μg/mL IgG
20 μg/mL anti-vimentin
40 μg/mL anti-vimentin
80 μg/mL anti-vimentin

Suppl. Figure 1

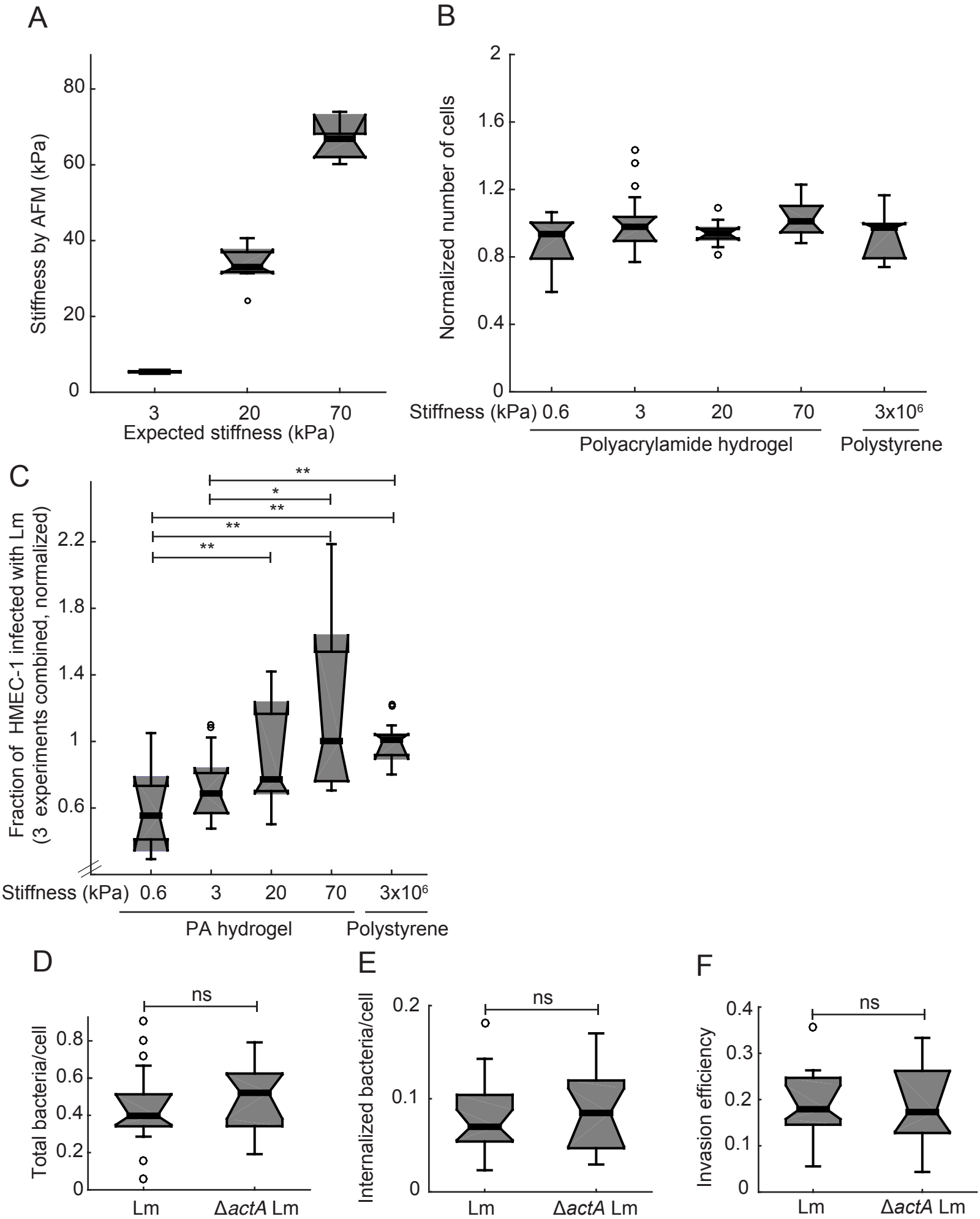

Suppl. Figure 2

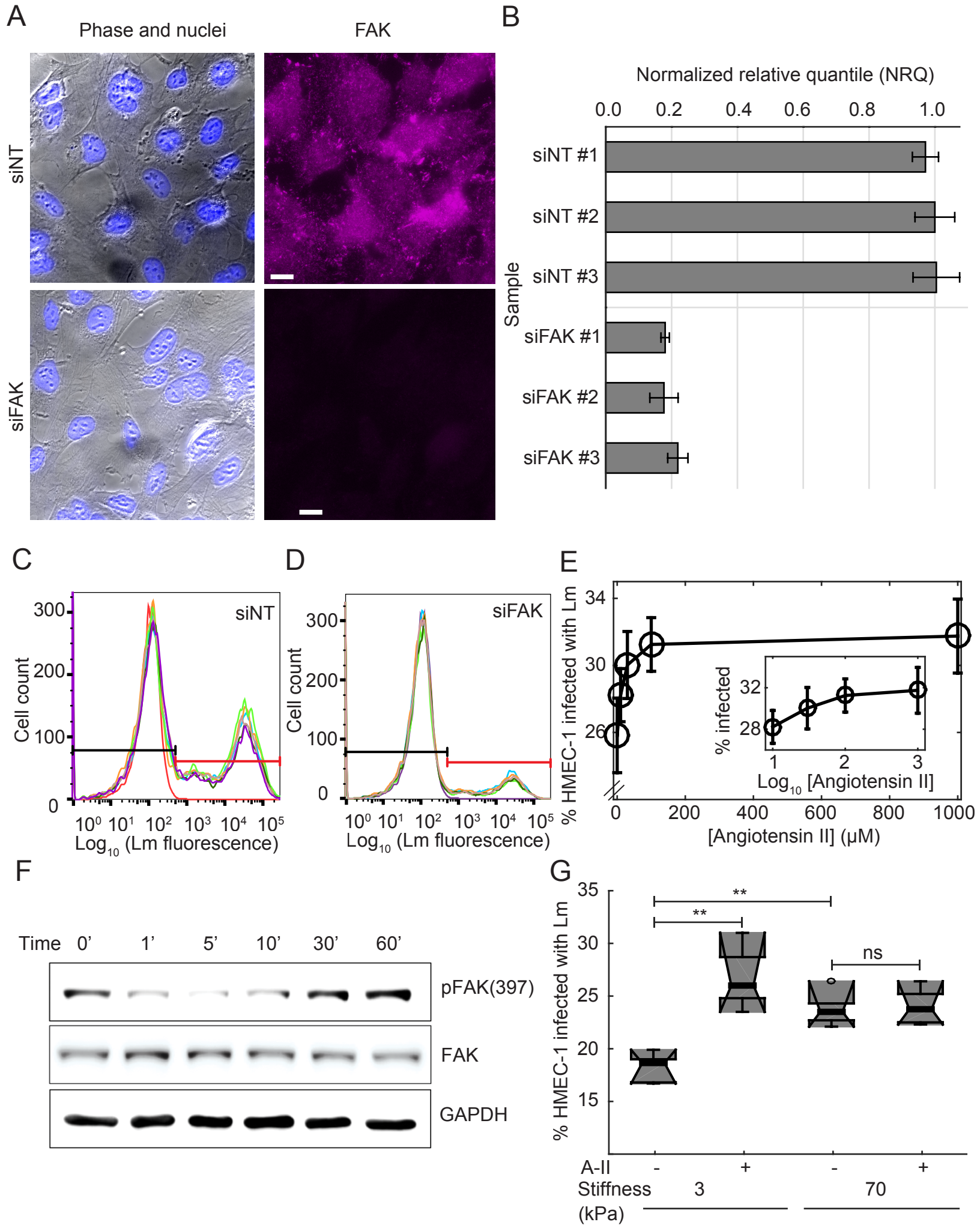

Suppl. Figure 3

A

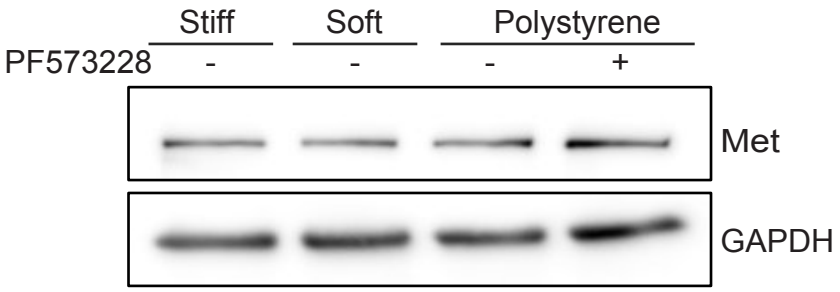

B

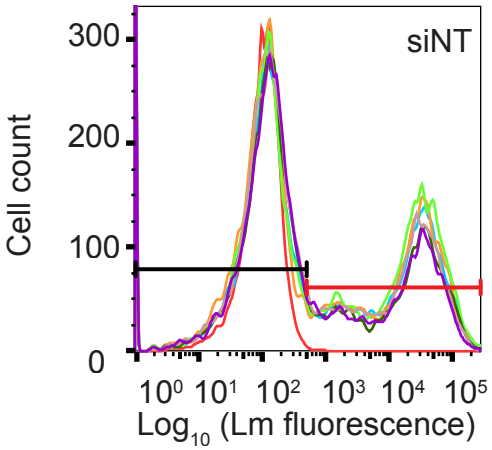

C

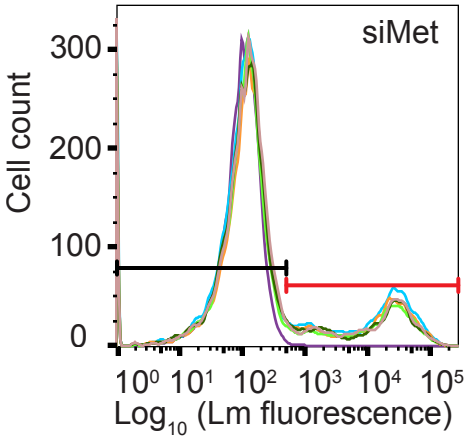

D

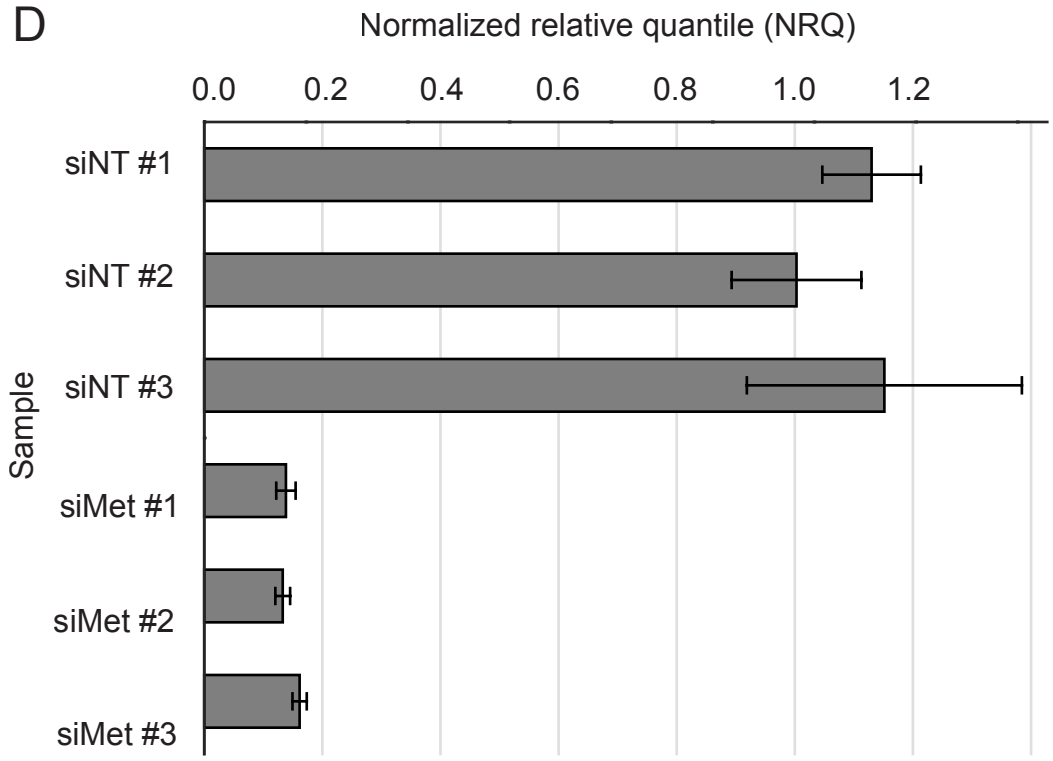

E

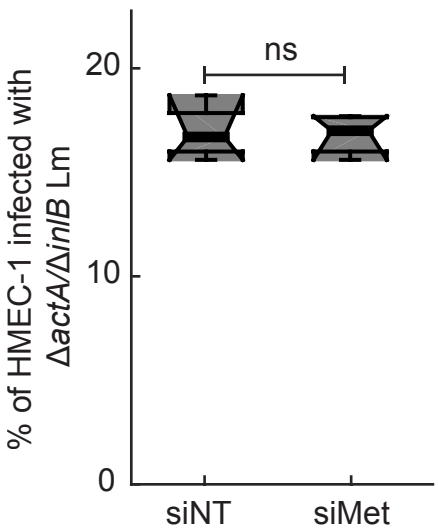

Suppl. Figure 4

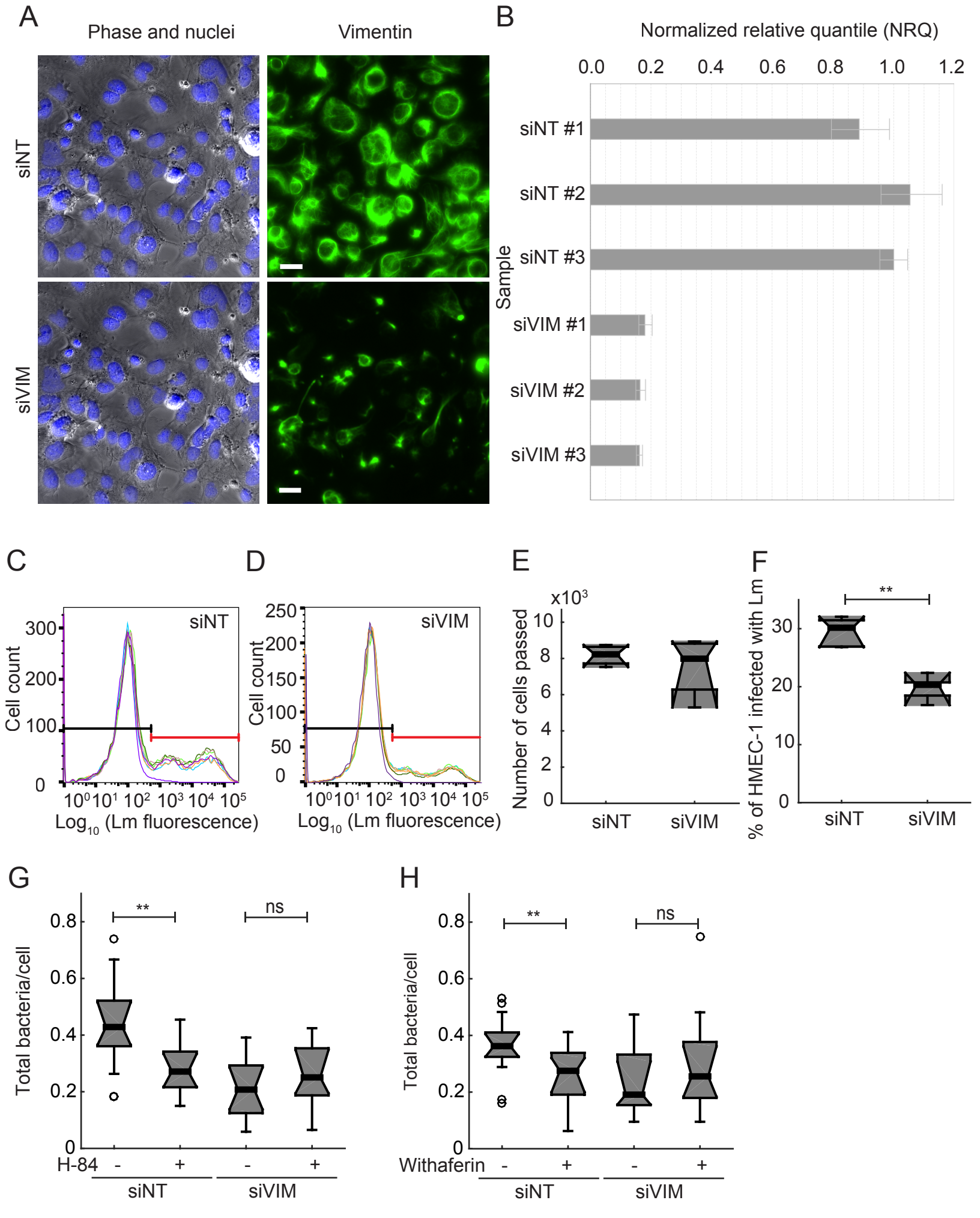

Suppl. Figure 5

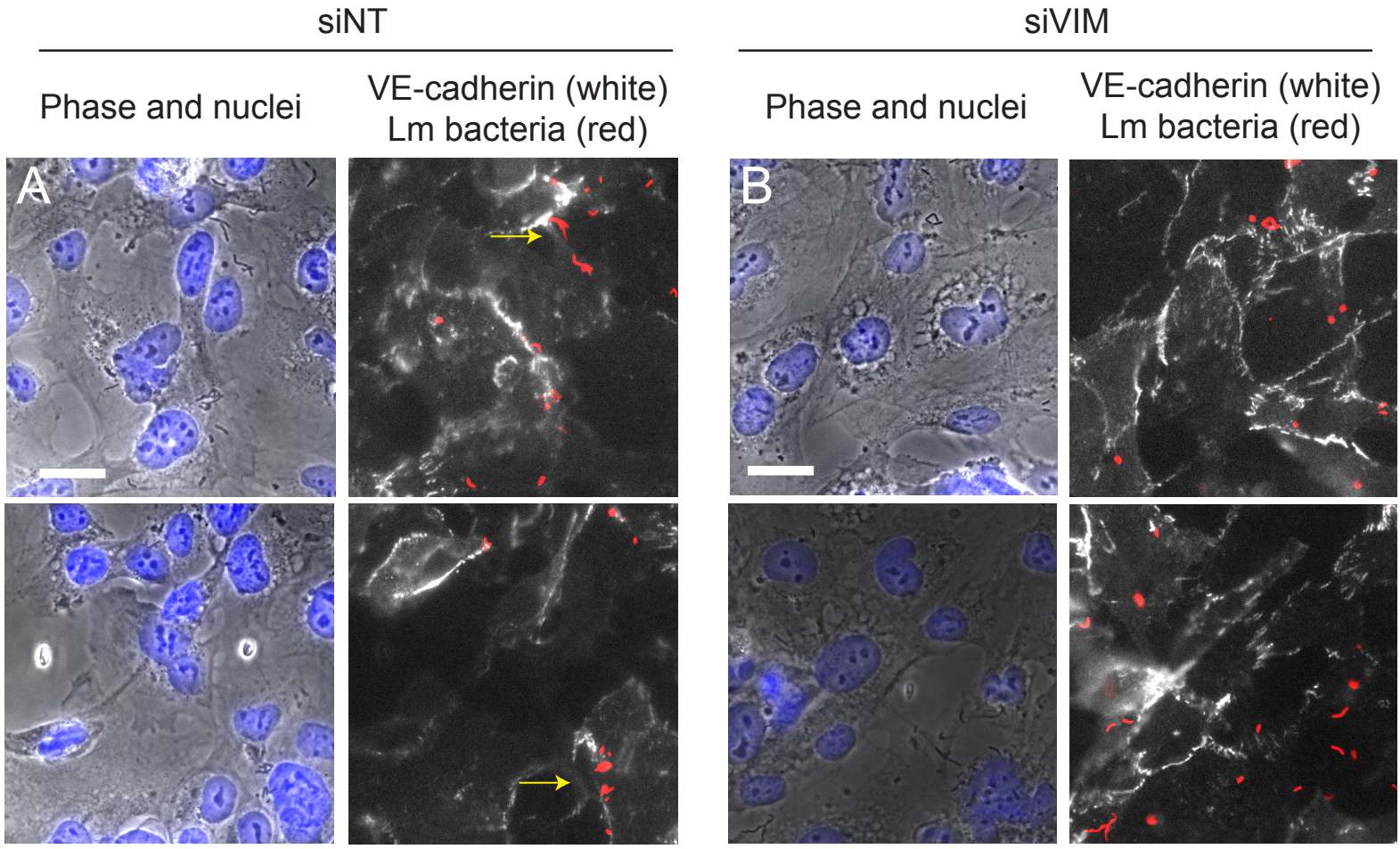

Supplementary Table 1: Bacterial strains used in this study

Name and source	Species	Genotype/Description
JAT983 (100)	*L. monocytogenes* 10403S	LLO^{G486D} actAp::mTagRFP
JAT985 (100)	*L. monocytogenes* 10403S	LLO^{G486D} *ΔactA* actAp::mTagRFP
JAT1045 (100)	*L. monocytogenes* 10403S	LLO^{G486D} Consitutive sGFP
JAT1046 (100)	*L. monocytogenes* 10403S	LLO^{G486D} *ΔactA* Consitutive sGFP
JAT1063 (100)	*L. monocytogenes* 10403S	LLO^{G486D} *ΔactA*/*ΔinlB* actAp::mTagRFP
JAT1060 (100)	*L. monocytogenes* 10403S	LLO^{G486D} *ΔinlB* Consitutive sGFP
JAT1051 (100)	*L. monocytogenes* 10403S	LLO^{G486D} *ΔinlA* actAp::mTagRFP
JAT1062 (100)	*L. monocytogenes* 10403S	LLO^{G486D} *ΔinlB* actAp::mTagRFP
JAT1115 (100)	*L. monocytogenes* 10403S	LLO^{G486D} *ΔinlF* actAp::mTagRFP
JAT638 (DP-L392) (85)	*L. innocua*	

Supplementary Table 2: Synthetic siRNA pools used in this study

Accession number	Gene (Protein)	Product Name	Catalog Number
	Negative control	ON-TARGETplus Non-Targeting Pool	D-001810-10
NM_000942	siGLO	ON-TARGETplus siGLO Control Reagent	D-001610-01
NM_004523.3	Kif11	ON-TARGETplus Human KIF11 (3832) siRNA	L-003317-00-0005
NM_003380.3	VIM	ON-TARGETplus Human VIM	L-003551-00-0005
NM_000245.3	MET	ON-TARGETplus Human MET	L-003156-00-0005
NM_001199649.1	PTK2 (FAK)	ON-TARGETplus Human PTK2	L-003164-00-0005